Characterization of the CEL-MODY mouse – A new disease model for chronic pancreatitis

Ivan Abbedissen

This thesis is submitted in partial fulfillment of the requirements for the degree of Master of Science

Department of Biological Science and

Department of Clinical Medicine

University of Bergen

Department of Medical Genetics

Haukeland University Hospital

June 2020

Table of contents

Acknowledgments

I would like to sincerely thank the greatest supervisors of all time; Karianne Fjeld, Anny Gravdal, and Anders Molven. With your experience and knowledge, this project has been orchestrated to fulfil all my expectations and more. Since the first day, I have felt welcome by your kind hearths and enthusiasm towards my success. You have shown faith in me by giving me responsibility and the possibility to thrive as a student.

Karianne, you have been a wonderful supervisor and motivator for me during our year together. The care you have shown for me has been cherished. You have always been available, motivating and helping me when I have been stuck or stressed. Thank you for all you have done.

Anny, I could not have wished for a better co-supervisor. You have always helped me when I needed it and been a great team-player. Thank you for teaching me how to run experiments and dissect mice, and of course, thank you for being patient with me and allowing me to take part in your precious mouse project.

Anders, you have been a great inspiration for me. Your knowledge has helped me understand both smaller details and the bigger picture of this project. Thank you for your counselling and support.

Furthermore, I would like to thank Khadija El Jellas for teaching me immunohistochemistry and helping me evaluate my results, our talks have been interesting and motivating. I wish to thank Marie Solheim and Bente Johansson for helping me with the mice, it has been a challenge to organize all the experiments and your help has been greatly appreciated. Solrun Steine, thank you for all the help with genotyping and our positive talks. I would like to thank my co-student Helene Pettersen for helping me with western blotting and always cheering me up by our fun conversations. Also, thanks to all the people at the Department of Medical Genetics and Department of Pathology, Haukeland Univeristy Hospital who have been helping me.

At last, I would like to thank my family and friends for supporting me throughout this master project, I could not have done it without you. A special thanks to my dear Andrea for supporting me every day. You have pushed me in times I needed motivation and praised me for my accomplishments.

Bergen, June 2020

Ivan Abbedissen

Abbreviations

ADM	Acinar-to-ductal metaplasia
bp	base-pairs
CEL/*CEL*	Carboxyl ester lipase/gene
CELP	Carboxyl ester lipase pseudogene
CEL-HYB/*CEL-HYB*	Carboxyl ester lipase hybrid/gene
CO_2	Carbon dioxide
CP	Chronic pancreatitis
CPA1/*CPA1*	Carboxypeptidase A1/gene
DNA	Deoxyribonucleic acid
ER	Endoplasmic reticulum
kb	Kilo bases
kDa	Kilo Daltons
MODY	Maturity-Onset Diabetes of the Young
PDAC	Pancreatic ductal adenocarcinoma
PRSS1	Cationic trypsinogen gene
RT	Room temperature
TGF-beta	Transforming growth factor beta
VNTR	Variable number of tandem repeats
~	Approximately

Abstract

Carboxyl ester lipase (CEL) is a digestive enzyme produced by the acinar cells of the pancreas. Two single-base deletion variants of the *CEL* gene cause a frameshift in the variable number of tandem repeats region located in the last exon. These *CEL* variants lead to a syndrome of pancreatic exocrine dysfunction and diabetes, known as Maturity-Onset Diabetes of the Young (CEL-MODY).

To get new insight into the disease mechanisms of CEL-MODY, our research group has developed a novel CEL-MODY knock-in mouse model. The overall aim of this project was to characterize this model. More specifically, we wanted to study the effect of the CEL-MODY protein at an organ level, with regard to pancreatic exocrine and endocrine dysfunction.

The CEL-MODY mice showed signs of pathological changes in the pancreas at 3 months of age, while severe, irreversible changes were observed at 6 months of age for both males and females. We observed exocrine atrophy, fibrosis and fatty infiltration, which are well known features of chronic pancreatitis (CP). Immunostaining indicated loss of Cel expression in atrophic exocrine tissue. We also detected signs of Cel protein aggregation, suggesting that CEL-MODY cause disease through the misfolding-dependent pathway of CP. No signs of diabetes were observed at 6 months of age, indicating that the islets of Langerhans remain functional in our mouse model, despite severe exocrine damage.

In summary, we found that the CEL-MODY mice developed spontaneous CP, making this the first mutant lipase mouse model for CP. However, the mice did not present any signs of diabetes development at 6 months of age.

1 Introduction

1.1 The pancreas

The human pancreas is an organ located in the upper abdomen surrounded by other organs such as the stomach, small intestine, kidney and spleen. This gland consists of an exocrine and an endocrine part that have two major functions vital for food digestion and blood glucose regulation, respectively. The pancreas is divided into three main anatomical areas, the head, body and tail (Figure 1.1 A).

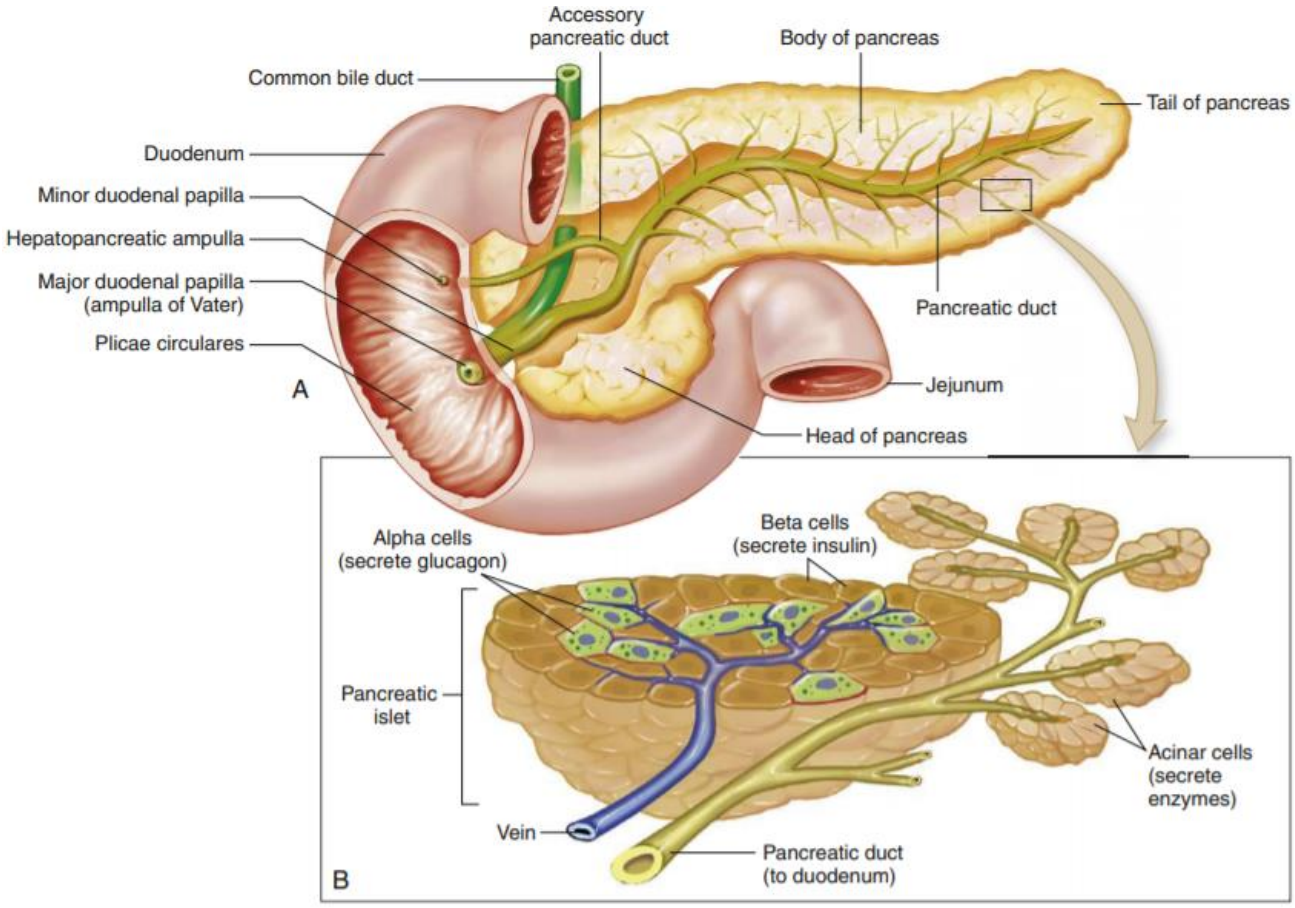

Figure 1.1. Overview of the anatomical areas of the pancreas*. A) The pancreas is divided into three anatomical areas, the head, body and tail, where the tail is more distal, and the head is proximal relative to the torso. The head lies next to the duodenum with a twisted structure. There is a duct throughout the whole pancreas that merges with the common bile duct in the head region of the pancreas, making the major duodenal papilla that leads into the duodenum. Within the pancreas, the main duct branches out into multiple smaller ducts. B) The acinar cells are arranged around smaller ducts in which they secrete digestive enzymes. Alpha and beta cells make up the major type of cells in the pancreatic islets that secrete hormones into the blood stream. Taken from: Copstead and Banasik, Pathophysiology, 5th ed, 2013, p 742.*

1.1.1 The exocrine pancreas

About 90 % of the pancreas is made of exocrine tissue, including acinar and ductal cells (Pandiri, 2014). The parenchyma of the pancreas has lobe structures where acinar cells make up branched grape-like structures called acini (Figure 1.1 B). Each acinus has a similar orientation of dipole acinar cells laying around a lumen with their apical part towards this lumen. All acini are connected to intralobular ducts that leads to larger interlobular ducts, which further merges with the main pancreatic duct (Longnecker, 2014). In addition, the common bile duct from the gallbladder merges with the pancreatic duct, supplementing bile salts to the duodenum. The ductal secretion is called pancreatic juice and consists of water, bicarbonate and digestive enzymes (Longnecker, 2014).

The pancreas can produce 1-2 litres of pancreatic juice every day (Jun et al., 2016). Production and secretion of bicarbonate is stimulated by the hormone secretin. Bicarbonate has an important role in neutralizing the pH in the duodenum which allows digestive enzymes to function in an optimal environment (Afroze et al., 2013).

In the acinar cells, inactive and partially active digestive enzymes are budding off from the Golgi network in vesicles called zymogen granules, before being secreted via exocytosis from the apical part of the cell and into the ductal lumen (Motta et al., 1997). The zymogen granules carry multiple types of digestive enzymes as listed in Table 1.1. Secretion of digestive enzymes are stimulated by several signalling molecules. The most common are cholecystokinin, a gastrointestinal hormone, and acetylcholine, a neurotransmitter that stimulates calcium mobilization leading to exocytosis of zymogen granules (Matthews et al., 1973).

Table 1.1. The most common digestive enzymes secreted by the pancreas.

Digestive enzyme	Biological Function	Reference
Proteases	Digest peptides	
Chymotrypsin (B, C)	Endopeptidase, cleaves peptide bonds after aromatic amino acid residues.	(Tomita et al., 1989, Batra et al., 2013)
Carboxypeptidase (A, B)	Exopeptidase, cleaves aromatic and basic amino acids from c-terminus.	(Laethem et al., 1996)
Elastase	Endopeptidase, cleaves peptide bonds after small uncharged amino acid residues.	(Szabó et al., 2016)
Trypsin	Endopeptidase, cleaves peptide bonds after basic amino acid residues.	(Scheele et al., 1981)
Lipases	Digest lipids	
Pancreatic triglyceride lipase	Cleaves ester bonds at sn-1 and sn-3 of triglycerides.	(Lowe, 1997)
Phospholipase A2	Cleaves sn-2 acyls ester bond of phospholipids.	(Gudgeon et al., 1991)
Pancreatic lipase related protein 2	Cleaves ester bonds of triglycerides, galacto- and phospholipids.	(Eydoux et al., 2008)
Carboxyl ester lipase (CEL)	Cleaves ester bonds of triglycerides, phospholipids, vitamin ester, cholesterol ester and fatty acids of hydroxyl fatty acids.	(Johansson et al., 2018)
Amylase	Digest carbohydrates	
Pancreatic alpha-amylase	Hydrolyses starch and glycogen.	(Brayer et al., 1995)
Nucleases	Digest nucleotides	
Deoxyribonuclease and ribonuclease	Cleaves the nucleic acids of DNA and RNA	(Chen, 2018)

1.1.2 The endocrine pancreas

Within the parenchymal lobes, distinct spherical groups of cells known as the islets of Langerhans are present (Figure 1.1 B). The islets comprise the endocrine pancreas, making up approximately 2 % of the organ (Murakami and Fujita, 1992) and consists of alpha, beta, gamma, delta and epsilon cells. The insulin producing beta cells make up the largest portion of the islets (~60%), followed by glucagon producing alpha cells (~30%) and the remaining 10 % is divided between delta, gamma and

epsilon cells, producing somatostatin, pancreatic polypeptide and ghrelin, respectively (Ionescu-Tirgoviste et al., 2015).

Insulin and glucagon are the two hormones important for maintaining glucose homeostasis in the body. When blood glucose rises after a meal, the beta cells are stimulated to produce insulin. Intracellular calcium stimulates secretion of insulin granules out into the blood (Mann and Bellin, 2016). Insulin migrates in the blood veins and binds to its responding receptors at different periphery tissues, such as the muscle, liver and fat, thereby stimulating glucose uptake. The secretion of insulin keeps the blood glucose from elevating too high (Mann and Bellin, 2016).

In contrast to insulin, glucagon up-regulates the blood glucose levels. When blood glucose is too low, alpha cells are stimulated to secrete glucagon into the bloodstream. Glucagon initiates liver glycogenolysis and gluconeogenesis, raising blood glucose to avoid hypoglycemia (Jiang and Zhang, 2003).

1.2 Pancreatic diseases

1.2.1 Diabetes mellitus

Diabetes mellitus is a group of metabolic disorders characterized by chronic hyperglycemia (Kharroubi and Darwish, 2015). In 2014, 8.5 % of adults worldwide were diagnosed with diabetes (World Health Organization, 2016). The two most common types are Type 1 Diabetes (T1D), accounting for around 5-10 % of diabetes cases, and Type 2 Diabetes (T2D), accounting for about 90 % of diabetes cases (Goyal and Jialal, 2020). Other forms of diabetes are gestational and monogenic diabetes.

T1D is an autoimmune disease that leads to destruction of the insulin producing beta cells (Bluestone et al., 2010). This disease mostly develops before the age of 20 (Maahs et al., 2010). One of the predominant genetic risk factors involve beta cell genes encoding antigen presenting molecules, causing an immune response (Concannon et al., 2009).

The hallmark for T2D is insulin resistance, i.e. that the insulin targeted cells do not respond efficiently to the hormone. Age of onset is typically after 40 years of age (American Diabetes Association, 2014). However, with lifestyle risk factors such as obesity, physical inactivity and energy-dense diet, an increasing number of younger people are diagnosed with T2D (Pulgaron and Delamater, 2014).

Gestational diabetes is defined as glucose intolerance with onset or first recognition during pregnancy (American Diabetes Association, 2014). Around 7 % of pregnant women get this form of diabetes, although for most of them, it disappears after giving birth.

Monogenic diabetes is caused by mutations in a single gene. A prevalence study from Norway found that 1.1 % of all patients in the Norwegian Childhood Diabetes Registry had monogenic diabetes (Irgens et al., 2013). Monogenic diabetes can be further sub-categorized into Maturity-Onset Diabetes of the Young (MODY), neonatal diabetes, syndromic diabetes and mitochondrial diabetes (Molven and Njolstad, 2011). MODY is the most common type of monogenic diabetes, characterized by autosomal dominant inheritance with neither beta cell autoimmunity nor insulin resistance. It usually leads to diabetes before 25 years of age (Urakami, 2019). Due to a relatively early onset and no insulin resistance, in addition to no beta cell autoimmunity, MODY is often misdiagnosed as T1D and T2D, respectively (Kavvoura and Owen, 2019). Today, 14 subtypes of MODY have been discovered (Urakami, 2019). The most common forms are caused by mutations in the hepatocyte nuclear factor 1, hepatocyte nuclear factor 4 and glucokinase. Mutations in the carboxyl ester lipase gene, causing MODY8 or CEL-MODY, are described in section 1.5.1.

1.2.2 Pancreatitis

Pancreatitis is defined as inflammation of the pancreas. It can either be acute, which has a sudden onset and short duration, or chronic, which develops gradually and results in irreversible organ damage (Banks et al., 2010). Pancreatitis is a complex disease with multiple risk factors where environment, anatomy and genetics play an important role (Hegyi et al., 2020). If not reversible, acute, recurrent acute and chronic pancreatitis form a disease continuum (Mayerle et al., 2019).

Acute pancreatitis (AP) can be divided into three stages: mild, moderate and severe depending on the presence and recurrence over a period (>48 hours) of organ failure and local or systemic complications (Banks et al., 2013). The most common cause of AP is obstructive (*e.g.* gallstone) and alcohol related (Chatila et al., 2019). Obstructive AP leads to retention of pancreatic juice drainage, but can be cured with fasting and by removing the blockage (Banks et al., 2013). Alcohol abuse is believed to sensitise acinar cells for cholecystokinin, thereby increasing the secretion of digestive enzymes which can build up and cause premature activation (Wang et al., 2009). In addition, alcohol can disrupt calcium influx in the ducts, leading to calcification that partially obstructs drainage of pancreatic juice (Whitcomb, 2012). Retention of pancreatic juice can lead to inappropriate activation of digestive enzymes, causing autodigestion within the pancreas. If not reversed or if it recurs, AP can progress into chronic pancreatitis (CP).

CP is characterized by progressive parenchymal fibrosis, maldigestion, diabetes mellitus and pain (Etemad and Whitcomb, 2001). Progressive pancreatic inflammation and necrosis results in loss of both exocrine and endocrine tissue. Known risk factors for CP are classified into: toxic-metabolic; genetic; autoimmune; recurrent and severe acute pancreatitis; obstructive; and idiopathic (Pham and Forsmark, 2018). How genetics play a role in CP will be described further in section 1.3.

1.2.3 Pancreatic cancer

Pancreatic cancer has the seventh highest mortality rate of all cancer types worldwide and the fourth highest in the United States (Rawla et al., 2019, Siegel et al., 2019). It can arise from both the exocrine and endocrine part of the pancreas. However, over 90 % of pancreatic cancers are adenocarcinomas arising from the exocrine gland (Hidalgo et al., 2015). Pancreatic neuroendocrine cancer is less common (<5 %) (Rawla et al., 2019). Some risk factors for pancreatic cancer are smoking, diabetes, alcohol, genetics and pancreatitis (Dhar et al., 2015).

Pancreatic ductal adenocarcinoma (PDAC) is a malignant tumour with a duct-like phenotype (Orth et al., 2019). A progression model has been characterized by an initial transition from normal pancreatic acinar cells into duct-like cells, termed acinar-to-ductal metaplasia (ADM) (Chuvin et al., 2017). ADM is induced by transforming growth factor beta (TGF-beta) signalling (Chuvin et al., 2017), typically observed as a consequence of stress from pancreatic inflammation and organ injury in pancreatitis (Murtaugh and Keefe, 2015). Furthermore, pro-oncogenic mutations induces ADM to become pre-invasive precursor lesions termed pancreatic intraepithelial neoplasia (PanIN) (Orth et al., 2019). Eventually, a gradual accumulation of mutations in tumour suppressor genes causes the PanINs to become invasive PDAC (Orth et al., 2019, Rawla et al., 2019).

1.3 Pathways of genetic risk in chronic pancreatitis

Progression from recurrent AP into CP can be driven by genetic factors (Mayerle et al., 2019). CP patients can have a complex set of genetic alterations that interplay with each other as well as other risk factors such as alcohol (Whitcomb, 2012). Today, three pathological pathways are described in genetically driven CP (Mayerle et al., 2019).

1.3.1 The trypsin-dependent pathway

Trypsin plays a major pathological role in pancreatitis, by premature activation and driving the progression of disease through its ability to activate other digestive enzymes inside the pancreas (Mayerle et al., 2019). Certain autosomal dominantly inherited mutations in the cationic trypsinogen gene (*PRSS1)* causes hereditary pancreatitis (Mayerle et al., 2019). Gain-of-function mutations can increase PRSS1s ability to autoactivate prematurely before entering the duodenum (Hegyi and Sahin-Tóth, 2017).

Other genetic risk factors are variants of serine protease inhibitor Kazal type 1 (*SPINK1*) and chymotrypsin C (*CTRC*) (Muniraj et al., 2014). In general terms, they manage trypsin inhibition and trypsinogen degradation, respectively. Pancreatic secretory trypsin inhibitor (encoded by *SPINK1*) inhibits trypsin and is up-regulated during inflammation (Muniraj et al., 2014). Loss-of-function mutations in *SPINK1* impairs this inhibition of active trypsin. Too high calcium levels or loss-of-function mutations inhibit CTRCs degradation capacity of inactive trypsinogen (Muniraj et al., 2014).

1.3.2 The misfolding-dependent pathway

More recently, an alternative pathway to premature trypsin activation has been identified. In common for the genes involved is that they encode misfolding proteins that lead to protein aggregation, impaired secretion, increased endoplasmic reticulum (ER)-stress, and eventually apoptosis (Sahin-Toth, 2017). The pathway is named the misfolding-dependent pathway of genetic risk in CP and certain mutations in the digestive enzymes such as PRSS1, carboxypeptidase A1 (CPA1) and carboxyl ester lipase (CEL) have shown to belong to this pathway (Whitcomb et al., 1996, Fjeld et al., 2015, Sahin-Toth, 2017). The role of CEL in CP is further described below.

1.3.3 The ductal pathway

The cystic fibrosis transmembrane conductance regulator (CFTR) stimulates duct cells to produce bicarbonate-rich fluid which contributes to flushing trypsin out of the pancreas (Muniraj et al., 2014), and mutation variants of the *CFTR* has shown to increase the risk of CP 4-fold (Mayerle et al., 2019). Furthermore, the calcium sensing receptor (CASR) regulates calcium influx in the duct cells. Alcohol and certain mutation variants of CASR leads to impaired function, causing calcification that may progress into CP (Mayerle et al., 2019).

1.4 Carboxyl ester lipase

Carboxyl ester lipase (CEL), also known as bile salt-stimulated lipase (Hernell and Olivecrona, 1974), or bile salt-dependent lipase (Abouakil and Lombardo, 1989), is a digestive enzyme (EC 3.1.1.13). CEL is mainly expressed by the pancreatic acinar cells and accounts for about 4 % of the protein content in the pancreatic juice (Lombardo et al., 1978). The enzyme is secreted as partially inactive before entering the duodenum. Here, CEL is stimulated by bile salts and can hydrolyse ester bonds in cholesterol esters, fat-soluble vitamins, tri-, di-, and monoacylglycerols and several fatty acid esters of hydroxyl fatty acids (Lombardo and Guy, 1980, Kolar et al., 2016). CEL is also expressed in lactating mammary glands and is secreted as a content of breast milk (Blackberg et al., 1985). During infancy, fat absorption is low, however, CEL from the breast milk helps infants compensate for the low endogenous fat absorption (Lindquist and Hernell, 2010).

1.4.1 The human *CEL* locus

The human *CEL* gene is located at chromosome 9q34.3 and is ~10 kb in size, consisting of 11 exons (Figure 1.2.) (Taylor et al., 1991). In the last exon, there is a variable number of tandem repeats (VNTR) region consisting of nearly identical segments of 33 bp (Higuchi et al., 2002). The number of repeats vary from 3-23 in humans, although several studies have shown that 16 repeats is the most common (Ræder et al., 2006, Torsvik et al., 2010, Dalva et al., 2017). About 11 kb downstream of the *CEL* gene, a *CEL* pseudogene (*CELP*) is located (Figure 1.2). Despite having a high sequence homology to *CEL*, *CELP* is missing exons 2-7 and it also includes a stop codon in the second exon (Lidberg et al., 1992, Madeyski et al., 1999). Due to the premature stop codon, *CELP* is not expected to be translated into a functional protein (Nilsson et al., 1993).

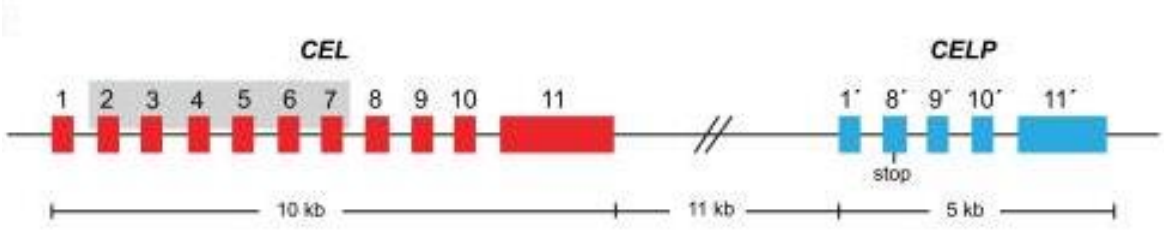

Figure 1.2. The human CEL locus. *In red, the 11 exons of CEL are shown spanning a sequence of about 10 kb. Further downstream, the CEL pseudogene is shown in blue. Marked in grey are the CEL exons 2-7 missing in CELP. The remaining 5 exons of CELP are named 1', 8', 9', 10' and 11' due to the sequence similarity with the corresponding exons in CEL. Note the stop codon in exon 8' in CELP. Figure taken from (Fjeld et al., 2015).*

1.4.2 The CEL protein

The most common human CEL variant with 16 VNTR repeats has a predicted theoretical protein size of ~79 kDa (Johansson et al., 2011). However, CEL is a glycoprotein that is heavily modified in the C-terminal tail. Therefore, the fully modified protein is detected with a molecular weight up to 120 kDa (El Jellas et al., 2018). The enzyme can structurally be divided into two parts, an N-terminal globular domain and an intrinsically disordered C-terminal domain (Figure 1.3). In the globular domain, there is an N-terminal ER-signalling sequence, a catalytic triad, multiple bile salt binding sites and a single site for N-glycosylation (Johansson et al., 2018). The C-terminal VNTR region is rich in proline (P), glutamic acid (E), serine (S) and threonine (T) residues, known as PEST-sequences, which are recognised for rapid protein degradation (Rogers et al., 1986). However, the same threonine and serine residues are serving as O-glycosylation sites, and it has been suggested that O-glycosylation of the CEL VNTR has a protective role by masking the PEST sequence, thereby prohibiting degradation of the enzyme (Wang et al., 1995, Bruneau et al., 1997).

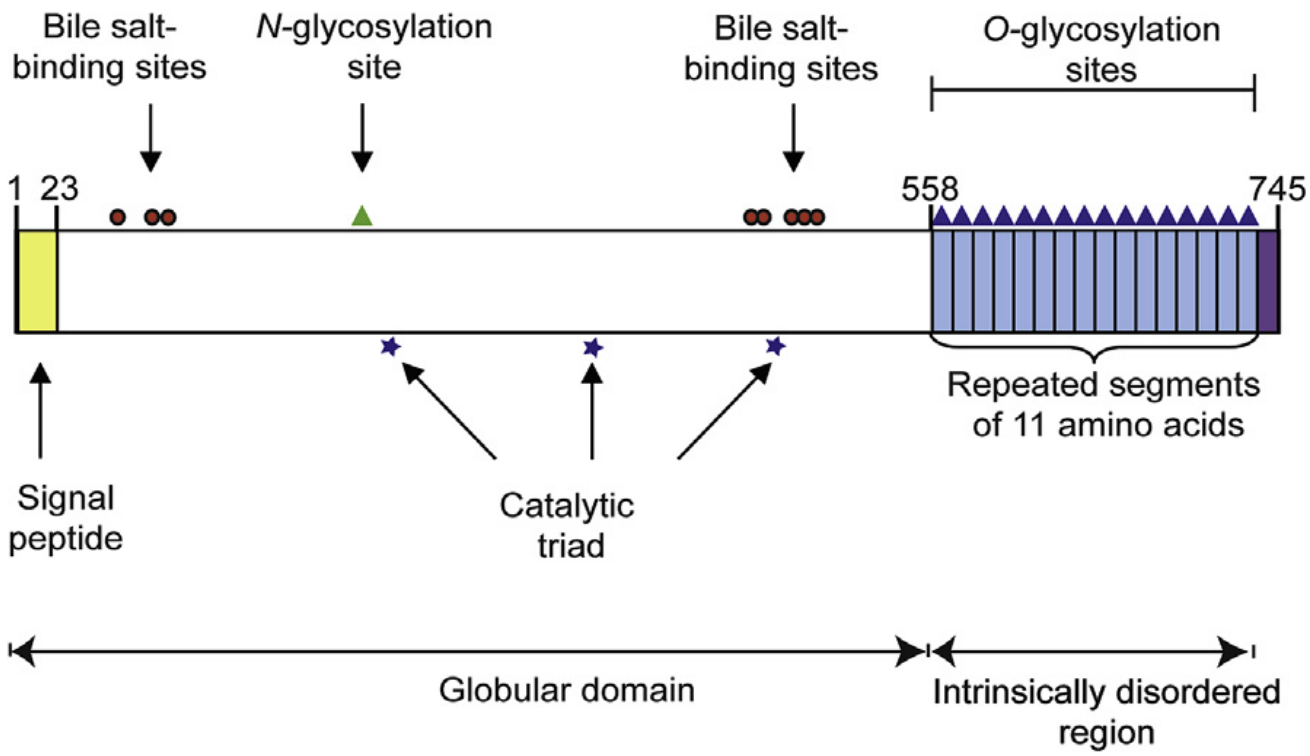

***Figure 1.3. Overview of the CEL protein structure**. A presentation of the protein with its functional parts indicated by arrows. The catalytic function is driven by three amino acids making a catalytic triad in the active site. Binding of bile-salts stimulates enzyme activation. O-glycosylation in the tail is believed to help with stability and secretion of the protein. This is a presentation of the 16-repeat variant, giving a 745 aa long protein. Figure taken from (Johansson et al., 2018).*

1.4.3 From translation to secretion

CEL follows the classical secretory pathway for digestive enzymes (Lombardo, 2001). The N-terminal ER-signalling peptide of CEL translocates the protein into the ER, where it is cleaved off and the protein is further modified. In the ER, the chaperone glucose regulated protein 94 aids in folding and glycosylation of CEL (Bruneau and Lombardo, 1995). Then, N-glycosylation of Asn210 occurs before CEL is transported to the Golgi network (Abouakil et al., 1993). Here, O-glycosylation occurs on the many serine and threonine residues of the VNTR region (Bruneau et al., 1997). Phosphorylation by casein kinase 2 on Thr340 is the final trigger for CEL to bud off from the Golgi, leaving the cell via exocytosis in zymogen granules (Pasqualini et al., 2000).

1.5 Pathological variants of CEL

1.5.1 CEL-MODY

In 2006, Ræder *et al.* reported that mutations in the *CEL* VNTR cause an autosomal dominantly inherited syndrome of endocrine and exocrine dysfunction (Ræder et al., 2006). The mutations were discovered in two families from the Western Norway. Their pedigrees revealed a family history of early onset diabetes, characterized as MODY, and the syndrome was named CEL-MODY or MODY8.

The CEL-MODY syndrome is caused by a single-base deletion in the first (DEL1) or fourth (DEL4) repeat of the VNTR. Both mutations lead to frameshifts, and the *CEL-MODY* variants encode truncated proteins due to a premature stop codon in the VNTR domain (Figure 1.4).

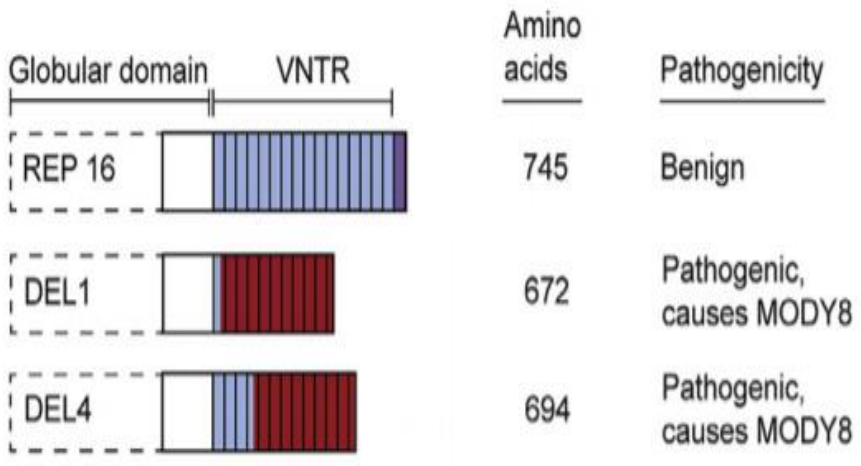

Figure 1.4. Presentation of the CEL protein tail in two deletion variants*. The REP 16 is illustrating a wild-type CEL VNTR with 16 repeats, each repeat indicated in blue boxes. Both DEL1 and DEL4 show a truncated tail, where the deletion causes an alternate tail indicated in red boxes. Note that DEL1 has a stop codon in repeat 11 while DEL4 has in repeat 13. Figure modified from (Johansson et al., 2018).*

CEL-MODY is a progressive disease with early exocrine dysfunction and lipomatosis (Ræder et al., 2006, 2007). Diabetes develops in the 40s and multiple pancreatic cysts have been observed in the diabetic patients (Ræder et al., 2014). In addition, one patient developed PDAC at a later stage in life (A. Molven, pers. Comm). The patients were first diagnosed due to their diabetes development. However, exocrine dysfunction is believed to be preliminary to diabetes, as exocrine dysfunction is also observed in nondiabetic CEL-MODY patients (Tjora et al., 2013). Based on these findings and the cellular studies discussed below, CEL-MODY seems to move more towards the area of CP, with diabetes development as a secondary consequence.

It is believed that the CEL-MODY syndrome is a gain-of-function disease where the mutant protein causes proteotoxic damage to the pancreas (Johansson et al., 2011, Torsvik et al., 2014, Xiao et al., 2016). Supporting this hypothesis, an earlier study of a CEL knock-out mouse model showed no significant signs of pancreatic disease development, demonstrating that loss of CEL can be tolerated (Vesterhus et al., 2010). Compared to the normal CEL protein, the CEL-MODY protein results in misfolding, impaired secretion and formation of both intra- and extracellular aggregates (Johansson et al., 2011, Torsvik et al., 2014). The aggregates cause ER-stress and induces apoptosis (Xiao et al., 2016). In addition, CEL-MODY proteins that have been secreted can be taken up again by adjacent cells and induce cell death (Torsvik et al., 2014, Dalva et al., 2020). The mutated protein has, in addition to a truncated tail, a totally different amino acid sequence in the tail region. This results in loss of multiple O-glycosylation sites and an increase in the local isoelectric point (pI) from 3.3 to 11.8 and overall pI from 5.2 to 9.5 (Johansson et al., 2011). Moreover, the presence of multiple cysteines caused by the frameshift may result in disulphide bridges that prevent proper folding of the protein, making it prone to aggregation (Xiao et al., 2016).

1.5.2 CEL-HYB

In 2015, Fjeld *et al.* reported that a hybrid variant of *CEL* (*CEL-HYB*) was a genetic risk factor for CP (Fjeld et al., 2015). This *CEL-HYB* variant was observed with a 5-fold frequency in idiopathic CP cases compared to controls in German and French cohorts.

CEL-HYB is most likely a result of nonallelic homologous recombination between *CEL* and *CELP* (Fjeld et al., 2015). The *CEL-HYB* allele is composed of exon 1-10 from *CEL* while exon 11 originates from *CELP*. The VNTR from *CELP* has a stop codon in repeat 3, which causes the CEL-HYB protein to be expressed with a truncated tail. When expressed in cell culture, CEL-HYB showed impaired secretion, intracellular retention, reduced enzymatic activity and induced cellular autophagy (Fjeld et al., 2015). Furthermore, there are unpublished data showing that CEL-HYB induces ER-stress, both

at the RNA and protein level (Tjora et.al., submitted). Based on these recent results, it is suggested that the *CEL-HYB* allele follows the misfolding-dependent pathway of genetic risk in CP (see section 1.3.2).

1.6 Mouse models for human disease

In medical research, the mouse has been a popular animal model for many years due to its genetic and physiological similarity to humans (Perlman, 2016). The most common laboratory mice today originates from the house mouse (*Mus musculus),* which has been used to develop inbred strains (Phifer-Rixey and Nachman, 2015). Inbred strains are generated by breeding siblings to create isogenic (genetically identical) mice. On average, 20 generations of inbreeding are sufficient to produce a population of mice that are about 99 % homozygous (Beck et al., 2000). Currently, over 400 inbred mice strains are available with one of the most popular being the C57BL/6 (Black 6) mouse (Benavides et al., 2019).

When the aim is to reproduce a human disease in mice, the strengths and weaknesses of a mouse strain needs to be thoroughly evaluated (Saloman et al., 2019). For instance, the Black-6 strain has substrains such as the C57BL/6J and C57BL/6N. In both substrains, multiple single nuclear polymorphisms have been identified that causes phenotypical differences (Simon et al., 2013). Knowing these differences are therefore very important when choosing a suitable strain for analysing human disease mechanisms and avoids the risk of interfering phenotypes. However, one of the advantages of using inbred strains is that the mice all have a uniform phenotype due to the isogenic background of the strain.

1.6.1 Genetically engineered mice

Developing genetically engineered mice based on human genetic diseases can serve as a good model to investigate the pathogenic mechanisms (Gurumurthy and Lloyd, 2019). Genome engineering allows for specific and sustainable alterations by either inserting, deleting or replacing DNA sequences that can cause a loss-of-function or a gain-of-function phenotype (Housden et al., 2017). Genetically engineered mice with foreign DNA is termed transgenic mice (Kumar et al., 2009). Typically, deleting or modifying a DNA sequence to remove a gene is termed knock-out (KO), and by inserting or replacing a DNA sequence to insert a gene is termed knock-in (KI).

1.6.2 Gene targeting by homologous recombination

To generate a transgenic KI mouse, gene targeting by homologous recombination is a technique that involves introducing recombinant DNA into embryonic stem (ES) cells by stable transfection (Figure 1.5 A) (Bouabe and Okkenhaug, 2013). A targeting vector is designed containing a selection marker for drug resistance and the recombinant DNA sequence of interest, flanked by sequences identical to the endogene sequence. These flanking sequences are termed homology arms (Ishii et al., 2014). In addition, the selection marker can be flanked by recombinase recognition sites for later deletion. The homology arms allow for homologous recombination, which is a natural process that can occur during meiosis or DNA repair where similar or identical DNA sequences are exchanged between two adjacent DNA strands (Gurumurthy and Lloyd, 2019). After homologous recombination, drug resistance allows for positive selection for the recombinant ES cells. A negative selection marker is included in the targeting vector, downstream of the homology arms, which can encode for toxic substance when homologous recombination has not occurred.

Next, the recombinant ES cells are injected into a blastocyst and implanted into a pseudo pregnant female by *in vitro* fertilization (Figure 1.5 B) (Gurumurthy and Lloyd, 2019). As the recombinant ES cells and native ES cells in the blastocyst originates from different mouse strains, pups are born as chimeras with different coat colour. The chimeric pups can then be used for further breeding with Cre expressing mice (Figure 1.5 C). Cre is a recombinase that recognize the loxP sites and cuts out the positive selection marker (Gurumurthy and Lloyd, 2019). The next generation of pups will then be heterozygous for the recombinant DNA.

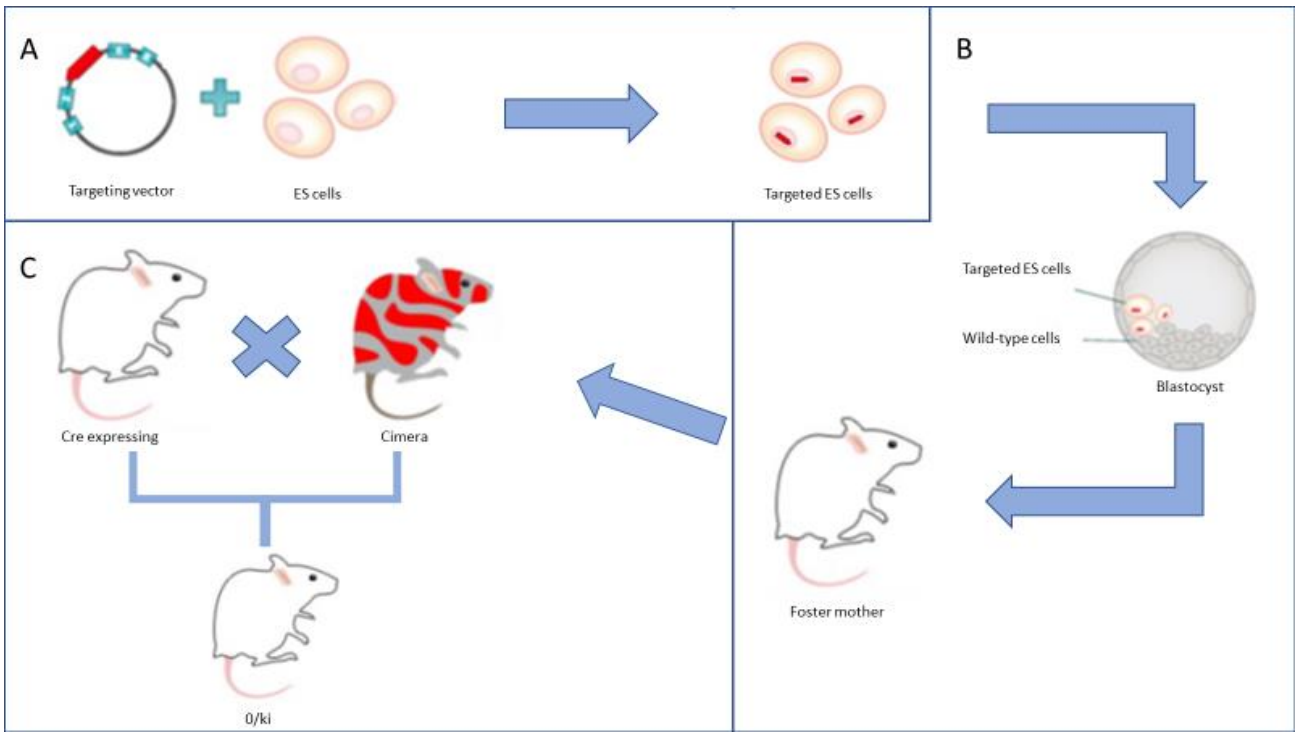

Figure 1.5. Overview of generating transgenic mice by gene targeting*. A) A vector is transfected into ES cells by electroporation. The vector contains an exogenous sequence marked in red, flanked by homology arms indicated in blue boxes. Selection markers allow harvesting of targeted ES cells that have incorporated the exogene via homologous recombination. B) The targeted ES cells are then injected into a blastocyst also containing wild-type ES cells. Further, this blastocyst is implanted into a pseudo pregnant female that gives rise to chimeric pups. C) A chimera pup where the targeted ES cells have contributed to the germ layer is used to crossbreed with a cre-expressing mouse, performing excision of the positive selection marker in the exogenous sequence. The litters from this breeding are heterozygous for the exogene, indicated as 0/ki.*

1.6.3 Constructing CEL-MODY and CEL-16R transgenic mice

Most research on CEL-MODY are based on cellular studies. To learn more about the disease mechanisms, our research group decided to develop a mouse model to be able to study CEL-MODY at the organ level. Previous mouse studies on CEL-MODY failed to show any pathological phenotype (Vesterhus et al., 2010, Ræder et al., 2013). However, neither of them used specific KI strategies for incorporating the human *CEL-MODY* VNTR into the endogenous mouse *Cel* locus.

The principle behind generating the new CEL-MODY mouse model was to exchange the endogenous mouse *Cel* VNTR region with the human *CEL-MODY* VNTR. Thereby, expression is still regulated under the endogenous *Cel* promotor.

Construction of the mouse model followed the techniques described above in section 1.6.2 and produced heterozygous CEL-MODY mice for human *CEL-MODY* VNTR (Figure 1.6). The *CEL-MODY* VNTR sequence was based upon a DEL1 mutation in a 14 VNTR repeat allele (Ræder et al., 2006).

In addition to the CEL-MODY mouse, we developed a CEL-16R mouse strain. Here the mouse *Cel* VNTR region was exchanged with the human *CEL* VNTR with 16 VNTR repeats. The purpose of this strain was to serve as a control for the normal human CEL protein. Since the mouse *Cel* gene harbours only 3 VNTR repeats (Holmes and Cox, 2011), the CEL-16R mouse will help us to separate any potential phenotypic effect that might originate from changing the mouse *Cel* VNTR *per se* from the specific effects induced by the *CEL-MODY* VNTR, thereby helping to better define the disease mechanisms.

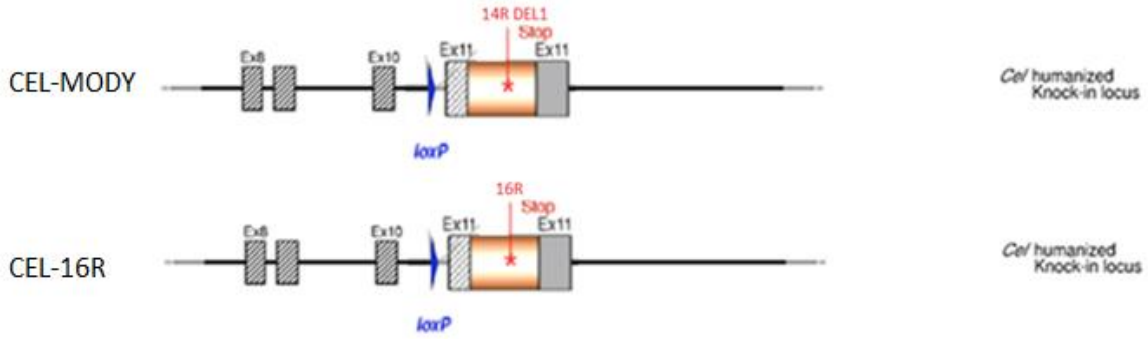

Figure 1.6. The CEL-MODY and CEL-16R humanized knock-in locus*. After gene targeting, generation of chimera and crossbreeding, two transgenic models were produced harbouring the human CEL-MODY VNTR and CEL-16R VNTR in exon 11, indicated by the red lines. One loxP site is left after Cre excision, indicated in blue.*

2 Aims of the study

The overall objective of this study was to learn more about the disease mechanisms of CEL-MODY by characterizing the phenotype of a new CEL-MODY mouse model.

The specific aims were:

- To determine whether expression of CEL-MODY causes chronic pancreatitis in mice
- If so, to determine whether CEL-MODY induced chronic pancreatitis causes subsequent development of diabetes

3 Materials

Table 3.1. Genotyping

Material	Catalogue number	Supplier
E.Z.D.A DNA tissue DNA kit	D3396-01	Omega Bio-Tek
Multiplex PCR Kit	206143	Qiagen
Tris-Borate-EDTA Buffer x10	A3945	PanReac, AppliChem
SeaKem LE Agarose	50004	Lonza
Ethidium Bromide (0.625 mg/ml)	E406-15ml	VWR
Gel Loading Buffer	G2526-5ML	Sigma Aldrich
100 bp DNA Ladder	N3231	New England Biolabs

Table 3.2. Pancreatic tissue lysis, SDS-PAGE and Western blot

Material	Catalogue number	Supplier
Trident RIPA lysis buffer	GTX400005	Gene Tex
cOmplete Protease Inhibitor Cocktail	11 697 498 001	Roche
Pierce BCA Protein Assay Kit	23225	Thermo Scientific
Phosphate-buffered saline	18912-014	Gibco
Tween 20	P9416	Sigma-Aldrich
NuPAGE LDS Sample Buffer (4x)	NP0008	Invitrogen
NuPAGE Sample Reducing Agent (10x)	NP0009	Invitrogen
NuPAGE 10% Bis-Tris Protein Gels, 1.0 mm, 10 well	NP0301BOX	Invitrogen
MagicMark XP Western Protein Standard	LC5602	Invitrogen
Precision Plus Protein Dual Color Standard	1610374	Bio-Rad
NuPAGE MOPS SDS Running Buffer (20X)	NP0001	Invitrogen
Blotting-Grade Blocker	1706404	Bio-Rad
Amersham Hybond P Western blotting membranes, PVDF	10600029	GE Healthcare
Methanol	67-56-1	Merck Millipore
Pierce ECL Plus Western Blotting Substrate	32132	Thermo Scientific

Table 3.3. CEL-immunostaining and trichrome staining

Materials	Catalogue number	Supplier
Dako Pen	S2002	Agilent Dako
SuperFrost Plus™ Adhesion slides	10149870	Thermo Scientific™
Target Retrieval Solution, pH 9.0, 10x	S2367	Agilent Dako
Protein block, Serum-free	X0909	Agilent Dako
Antibody Diluent, Background Reducing	S3022	Agilent Dako
Liquid DAB+ Substrate Chromogen System	K3468	Agilent Dako
Hematoxylin	S2020	Agilent Dako
Pertex Mounting Medium	00811-EX	Histolab
Ventana trichrome staining kit	860-031	Roche

Table 3.4. Antibodies

Antibody	Catalogue number	Supplier	Classification
Anti-CEL (rabbit polyclonal)	Gift	Gift from prof. Mark Lowe, Washington University School of Medicine, St. Louis, MO	Primary (WB)
Anti-β-actin (mouse monoclonal)	sc-47778	Santa Cruz Biotechnology	Primary (WB)
Anti-CEL (rabbit polyclonal)	HPA052701	Sigma Aldrich	Primary (IHC)
Goat anti-Rabbit IgG (H+L), HRP	656120	Invitrogen	Secondary (WB)
Donkey anti-mouse IgG-HRP	sc-2306	Santa Cruz Biotechnology	Secondary (WB)
MACH3 rabbit HRP-polymer detection kit	M3R531	Biocare medical	Secondary (IHC)

WB = Western blot, IHC = Immunohistochemistry

Table 3.5. Glucose homeostasis test

Materials	Catalogue number	Supplier
D -(+)-glucose	G8270	Sigma-Aldrich
Humulin NPH Insulin	ATC nr. A10A C01	Lilly
Freestyle Freedom Lite glucose meter		Abbot
Freestyle Lite test strips		Abbot

Table 3.6. Buffers and solutions

Solutions	Use	Composition
2 and 3 % agarose gel	Gel electrophoresis	2 or 3 % w/v SeaKem® LE Agarose dissolved in 1x TBE buffer and 1 µg/ml EtBr
Blotting buffer	Western blotting	1x NuPAGE Transfer Buffer and 10 % v/v methanol
PBS-T	Western blotting and CEL-immunostaining	Phosphate-buffered saline with 0,05 % v/v Tween 20
Blocking buffer	Western blotting	5% w/v Blotting-Grade Blocker in PBS-T
Antibody diluent	Western blotting	1% w/v Blotting-Grade Blocker in PBS-T
Glucose, 20%	IPGTT	20 % w/v D –(+)-glucose in physiological saline (3 % w/v NaCl) water
Insulin	IPITT	0.05-0.1 U/ml in physiological saline (3 % w/v NaCl) water

Table 3.7. Technical equipment

Instruments	Use	Manufacturer
Applied Biosystems Thermal Cycler 2720	Genotyping	Thermo Fischer Scientific
NanoDrop ND-1000	Genotyping	Thermo Fischer Scientific
Gel Doc EZ Imager	Genotyping and Western blotting	Bio-Rad
Infinite® 200 PRO	Western blotting	Tecan
Leica DM2000 LED	Histology	Leica Microsystems
Eppendorf Centrifuge 5417C	Genotyping and Western blotting	Applied Biosystems
Megafuge 1.0 R	Blood sampling	Heraeus Sepatech
XCell SureLock Mini-Cell Electrophoresis System	Western blotting	Thermo Scientific
XCell II Blot Module	Western blotting	Invitrogen

Table 3.8. Analytical software

Software	**Use**	**Supplier**
Microsoft Excel	Mouse body weight development, tissue weight and glucose homeostasis	Microsoft Corporation
GraphPad Prism	Mouse body weight development, tissue weight and glucose homeostasis	GraphPad Software, Inc
Leica Application Suite v2.0	CEL-immunostaining and trichrome staining	Leica Microsystems
Aperio ImageScope	HE-staining	Aperio Technologies

Table 3.8. Analytical software

Software	Use	Supplier
Microsoft Excel	Mouse body weight development, tissue weight and glucose homeostasis	Microsoft Corporation
Microsoft Power Point	Editing of figures	Microsoft Corporation
GraphPad Prism	Mouse body weight development, tissue weight and glucose homeostasis	GraphPad Software, Inc
Leica Application Suite v2.0	CEL-immunostaining and trichrome staining	Leica Microsystems
Aperio ImageScope	HE-staining	Aperio Technologies

4 Methods

4.1 Animals

The CEL-MODY and CEL-16R mouse strain were developed on a C57BL/6N background. For both strains, breeding was performed with CEL-MODY/CEL-16R heterozygote males and wild-type females at the Laboratory Animal Facility, Faculty of Medicine, University of Bergen. The mice followed a normal 12-hour day/night cycle and were fed normal chow diet. Both males and females were studied. The mice were divided into twelve cohorts determined by gender, age, strain and genotype (Table 4.1.). Each cohort had a minimum of 6 mice.

Table 4.1. Overview of cohorts studied.

Gender	**3 months**	**6 months**
Male	Control	Control
Male	CEL-MODY	CEL-MODY
Male	CEL-16R	CEL-16R
Female	Control	Control
Female	CEL-MODY	CEL-MODY
Female	CEL-16R	CEL-16R

4.2 Study approval

Both animal breeding and the plan for animal experiments were approved by Mattilsynet (Norwegian Animal Welfare Agency) in December 2017. FOTS ID numbers were 13902 and 13510.

4.3 Genotyping

4.3.1 DNA extraction

Tissue sampling by ear punches were done on two-week-old mice and used to identify the genotype. DNA was extracted from mouse tissue using the E.Z.N.A tissue DNA Kit according to the manufacturer's protocol. One exception was for lysis buffer treatment which was efficient after one treatment instead of two. The DNA concentration was measured using NanoDrop ND-1000.

4.3.2 Polymerase chain reaction (PCR)

First, a general PCR was performed for both CEL-MODY and CEL-16R strains to detect heterozygosity of the mouse *Cel* locus. Next, specific PCRs were set up to validate the presence of exogene *CEL-MODY* or *CEL-16R* VNTRs. PCR primer sequences are listed in Table 4.2. The PCR reaction was performed in a total volume of 25 µl and included 30-50 ng DNA, 1x Qiagen multiplex mastermix, 5 µM forward primer and 5 µM reverse primer. PCR programs used are listed in Table 4.3. and 4.4.

Table 4.2. Primers used for PCR genotyping

General PCR	***Primer sequence***
196271cre (fwd)	5'- GCA AAC TTC TTA TTT ATC CTC AAG CCT TGG -3'
196272cre (rev)	5'- GTT ATC GTC TTA GTG ATG TCC AGG TAG TTG C -3'
CEL-MODY specific PCR	
0017-TS/PNI (fwd)	5'- GCC AAA GAG ACA TGC AGT GAG AAG AGT ACC -3'
198280oth (rev)	5'- CGA ATG TCA CAG CCC AGA ACT TCA GG -3'
CEL-16R specific PCR	
0018-TS/PNI (fwd)	5'- CCA CCA TGA GTC CAA TGA TTG CAC C -3'
196274oth (rev)	5'- GGT GGC CTC CTG GTC GGT CAC T -3'

Table 4.3. PCR program for general genotyping

Step	Temperature	Time	Cycles
Pre-heat	95°C	15 min	-
Denaturing	94°C	60 sec	35
Annealing	65°C	90 sec	35
Extension	72°C	90 sec	35
Final extension	72°C	10 min	-
Hold	4°C	∞	-

Table 4.4. PCR program for CEL-MODY and CEL-16R specific genotyping

Step	Temperature	Time	Cycles
Pre-heat	95°C	15 min	-
Denaturing	94°C	30 sec	30
Annealing	65°C	30 sec	30
Extension	72°C	5 min	30
Final extension	72°C	8 min	-
Hold	4°C	∞	-

4.3.3 Agarose gel electrophoresis

For verification of the PCR products, 12.5 µl of PCR product was added 7.5 µl gel loading buffer and loaded on a 2 or 3 % agarose gel with TBE buffer and EtBr (1 µg/mL). Samples were loaded next to a 100 bp size marker and run at 90 V for one hour. Visualization of bands was done under UV-light using a Bio Rad Gel Doc EZ Gel Imager. The expected band sizes are listed in Table 4.5.

Table 4.5. Expected PCR product size after agarose gel electrophoresis.

General PCR	Expected band size
Wild-type	303 bp
Heterozygote	303 + 394 bp
Specific PCR	
Wild-type	No band
CEL-MODY	256 bp
CEL-16R	286 bp

4.4 SDS-PAGE and Western blotting

4.4.1 Preparation of mouse pancreas tissue lysates

Mice were sacrificed at seven-weeks and their pancreas harvested. The organ was immediately snap-frozen on liquid nitrogen. A small fraction of the pancreas was cut off and immediately put in 500 µl ice cold Trident RIPA buffer pre-supplemented with cOmplete Protease Inhibitor Cocktail (8.33 mM EDTA) and stored on ice. For homogenization, a pestle was used to stroke the tissue 10 times. The samples were then put on a rotary wheel for 20 min at 4°C. Further, the sample was centrifuged for 15 min at 13000 rpm at 4°C before separating the supernatant from the insoluble pellet. The supernatant fraction was further analysed as the pancreas lysate.

4.4.2 Protein concentration

The protein concentration of pancreas lysates was measured using Pierce BCA Protein Assay Kit according to manufacturer's protocol. The pancreas lysates were diluted 1:5 to fit within the protein standard concentration range. Protein concentration was then measured in Infinite 200 PRO at 562 nm.

4.4.3 SDS-PAGE

For preparation of samples, 10 µg of protein from pancreas lysate was incubated with 1x LDS Sample Buffer and 2x Sample Reducing Agent at 56°C for 15 min. The samples were loaded next to 4 µl Precision Plus Protein Dual Color Standard and 2 µl MagicMark XP Western Protein Standard onto a 10% Bis-Tris protein gel and separated by electrophoresis in a XCell SureLock Mini-Cell system. The gel was run in 1x MOPS buffer first at 90 V for 15 min, then 180 V until the migration front had run out of the gel.

4.4.4 Western blotting

The proteins were transferred from the SDS gel onto a PVDF-membrane. Prior to blotting, the hydrophobic membrane was prewetted in 100% methanol (1 min) to be compatible in aqueous solution, followed by a short rinse in distilled water (1 min). The blotting sandwich was made in XCell Blot Module system according to Invitrogen. Blotting was performed at 30 V for one hour. Next, the membrane was incubated in Blocking buffer for one hour at room temperature (RT). After blocking, the membrane was washed 3x5 min in PBS-T before incubation with primary antibodies

overnight at 4°C. The primary antibodies used were rabbit anti-CEL (1:10 000) and mouse anti-β-actin (1:2000 or 1:1000). Washing 3x5 min in PBS-T was done after incubation. The membrane was further treated with secondary HRP-conjugated anti-rabbit (1:5000) and anti-mouse (1:5000) respectively for one hour in RT. After incubation, the membrane was washed 3x5 min in PBS-T. ECL Plus Western Blotting Substrate was used for 5 min at RT before the chemiluminescent signal was detected using Bio Rad Gel Doc EZ Gel Imager.

4.5 Mouse body weight development

Weighing of the mice starting at eight weeks of age and continued every second week until the experimental end point at 14 or 28 weeks. It was performed consistently at the same time in the end of the week.

4.6 Mouse tissue and blood collection

At the experimental end point, tissues and blood samples were harvested. All mice were sacrificed by CO_2 euthanasia. Blood was collected post-mortem by cardiac puncture and incubated at RT for 30 min before centrifugation at 3000 rpm and 4°C for 10 min. The blood serum was separated from the plasma and stored at -80°C. Pancreas, liver, epididymal and subcutaneous white adipose tissue, muscle and brown adipose tissue were harvested. The tissues (except muscle) were weighed before being divided in two parts: one part stored in 4 % formaldehyde for histology/IHC analysis and the other part stored in liquid nitrogen for potential protein analysis. In this project, we only analysed the pancreas. Other tissues and blood samples were not investigated.

4.7 Histology of the mouse pancreas

4.7.1 Tissue preparation and Hematoxylin and Eosin (HE)-staining

After fixation in 4 % formaldehyde at RT overnight, mice pancreas specimens were embedded in paraffin and cut into 4-µm sections onto SuperFrost Plus Adhesion Slides, followed by incubation at 56 °C overnight. Embedding, sectioning and standard HE-staining were performed by the histology laboratory at the Department of Pathology, Haukeland University Hospital. After staining, the slides were scanned digitally and analysed using Asperio ImageScope.

4.7.2 CEL-Immunostaining

The pancreas tissue slides were baked at 56°C for at least 5 min before deparaffinizing in 100% xylene (2x5 min), 100 % ethanol (2x2 min), 96 % ethanol (2x2 min), 80 % ethanol (2 min) and distilled water (1 min with shaking). Epitope retrieval was done at 120°C in Target Retrieval Solution (pH 9.0) for 1 min using a pressure cooker. After retrieval, the slides were cooled at RT for 5 min before further cooling in running tap water. Next, the tissue slides were washed 3x5 min in PBS-T, blocked using Protein block for 10 min at RT, and further washed 3x5 min in PBS-T. For primary antibody incubation, rabbit anti-CEL (1:200, Sigma) was used at 4°C overnight in a humidity chamber. After incubation with primary antibody, the slides were washed 3x5 min in PBS-T before blocking of the peroxidase activity with 3 % H_2O_2 for 10 min at RT. Further, the slides were rinsed in distilled water for 1 min before being washed in PBS-T 3x5 min.

For detection with secondary antibody, tissues were incubated with MACH3 anti-rabbit probe for 20 min at RT, washed 3x5 min in PBS-T, then incubated with MACH3 anti-rabbit polymer for 20 min at RT. After polymer incubation, the tissues were rinsed in water for 1 min and washed 3x5 min in PBS-T. Substrate development was done with Liquid DAB+ Substrate Chromogen System for 3 min at RT. The reaction was stopped by dipping the slides in water, first rinsing and then washing for 2 min. Nucleus staining was done using Hematoxylin (Dako) for 10-20 min at RT before rinsing in running tap water for 2 min. The slides were then dehydrated 1 min in distilled water, 80 % ethanol, 96 % ethanol, 100 % ethanol and 2x2 min xylene before mounting with cover slips using Peritex Mounting Medium. Tissue slides were analysed with Leica DM2000 LED and Leica Application Suite v2.0. All washing steps were performed with shaking.

4.7.3 Trichrome staining

Trichrome Staining Kit (Ventana) was used to detect fibrosis. All solutions in the kit were ready to use, however, incubation times were optimized as described below. Baking and re-hydration of the tissue slides were done as described under 4.7.2. Tissue slides were treated with Bouin's solution at 50°C for 32 min in a humidity chamber before washing 3x2 min in distilled water. Nucleus staining was done by mixing reagents Hematoxylin A and B (1:1). The solution was applied to the slides, incubated for 4 min at RT, followed by washing 3x2 min in distilled water. For cytoplasm staining, Trichrome Red was applied for 6 min at 37°C and washed 3x2 min in distilled water. Trichrome Mordant was applied to removed excess red staining from collagen for 16 min at 37°C and followed by immediate addition of Trichrome Blue for collagen staining for 16 min at same temperature with no washing between. After collagen staining, the slides were washed 3x2 min in distilled water.

Trichrome Clarifier was applied for 3 min in RT before immediate dehydration in 80 % ethanol, 96 % ethanol and 100 % ethanol. The slides were then kept in xylene 2x2 min before mounting of cover slips using Pertex Mounting Medium. All slides were analysed as described in 4.7.2. Each washing step was performed with shaking.

4.8 Glucose homeostasis tests

4.8.1 Intraperitoneal glucose tolerance test (IPGTT)

Mice were fasted overnight for 14 hours in new cages. The mice were weighted before measuring blood glucose at time 0. The blood glucose was measured from a small cut by a razor on the distal part of the tail. All mice were kept in separate cages during the test. The glucose (20 %) was injected intraperitoneally into the posterior-distal part of the abdomen. Injection volume correlated with body weight (10 µl per gram body weight). After injection, blood glucose was measured with FreeStyle Freedom Lite glucose meter from the cut in the tail at time intervals of 15, 30, 60, 90 and 120 minutes.

4.8.2 Intraperitoneal insulin tolerance test (IPITT)

Mice were fasted for three hours (07.00 to 10.00) in new cages. Experimental procedures such as glucose measurements and injections were performed as described in section 4.8.1. Insulin concentrations used were different for the respective cohorts and listed in Table 4.6.

Table 4.6. Insulin concentration used for IPITT in each cohort.

Gender	Age	Insulin concentration (U/kg)
Male	6 months	1
Male	3 months	0.75
Female	6 months	0.75
Female	3 months	0.5

4.9 Statistics

Results were plotted as individual data points using GraphPad Prism 8 with the mean and standard error of the mean indicated. Differences of mean between two cohorts were analysed by unpaired t-test. $P < 0.05$ was considered statistically significant.

5 Results

In this study, we have analysed CEL-MODY mice and compared them to two control mice strains. One of the controls is the CEL-16R mouse model that express the normal human VNTR with 16 repeats. For both CEL-MODY and CEL-16R, we used heterozygous (0/ki) mice. In addition, we included control (0/0) mice from the breeding schemes of both CEL-MODY and CEL-16R mice. These are wild-type C57BL/6N mice and referred to as controls throughout this study.

5.1 Identification and verification of transgenic CEL mice

5.1.1 Genotyping of CEL-16R and CEL-MODY mice

Before starting our animal experiment, all mice were genotyped by a PCR assay. DNA was extracted from mouse tissue and used as template. For each mouse strain, the assay included two PCR reactions. First, a general PCR was performed to distinguish between heterozygous (0/ki) and control (0/0) mice. Next, a specific PCR was set up to amplify the exogenous VNTR region of either CEL-16R or CEL-MODY. The PCR products from each reaction were analysed by agarose gel electrophoresis and a typical genotyping result is presented in Figure 5.1. In the general PCR, a product with the size of 303 bp was expected for the wild-type allele, while an additional product of 394 bp was expected if the mouse carried one humanized *Cel* allele (see Methods, Table 4.5).

Genotyping results of four mice from each of the CEL-16R and CEL-MODY strains are presented in Figure 5.1. The results of the general PCR showed two bands in the agarose gel at around 300- and 400 bp for two CEL-16R mice and three CEL-MODY mice thus suggesting that these mice were heterozygous (Figure 5.1 A). In the remaining three mice, only one band at 300 bp was detected indicating control mice.

These genotyping results were verified by the specific PCR products showing one band at about 300 bp for the same five mice with two bands from the general PCR (Figure 5.1 B). The expected PCR product from amplifying an exogenous VNTR part from the CEL-16R mice was 286 bp, while 256 bp for the CEL-MODY mice (Table 4.5). No bands were observed for the control mice, as expected.

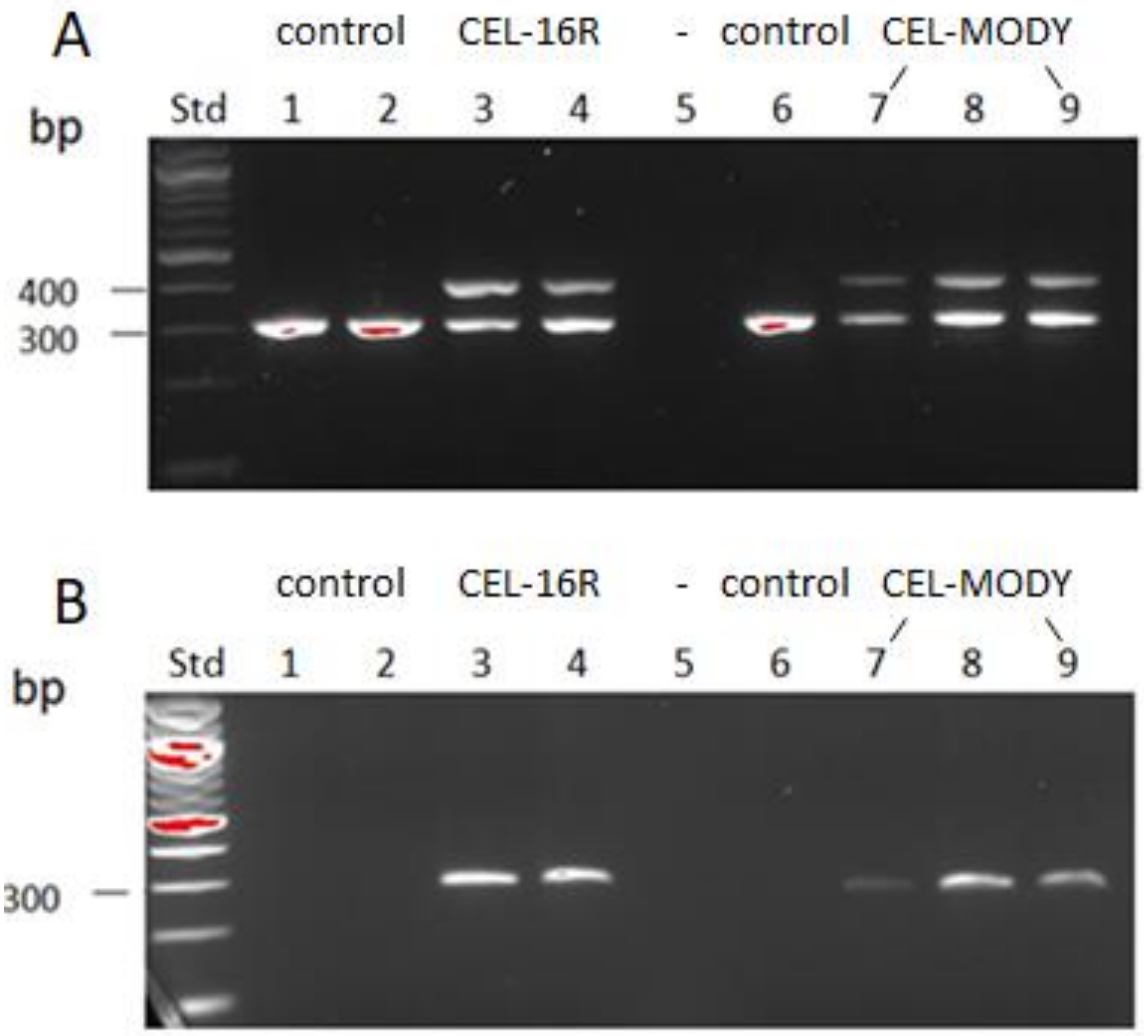

Figure 5.1. Genotyping results of CEL-16R and CEL-MODY mice. *PCR products were separated on a 2 % agarose gel stained with EtBr. Lane 1-4 represents genotyping of the CEL-16R strain and lane 6-9 represents genotyping of the CEL-MODY strain. The wells were loaded with 12.5 µl PCR product next to a DNA standard (std). Lane 5 was empty. A) Results from the general PCR. In lane 1, 2 and 6, one band was observed at 300 bp which showed that these are control (0/0) mice. Two bands were present at 300 and 400 bp in lane 3, 4 and 7-9, suggesting heterozygous (0/ki) mice. B) Results from the specific PCR. In lane 1, 2 and 6, no bands were detected, verifying the controls in A. Lane 3, 4 and 7-9 showed one band at about 300 bp, indicating CEL-16R (lane 3, 4) and CEL-MODY (lane 7-9) positive samples, respectively.*

5.1.2 Detection of humanized Cel proteins in CEL-16R and CEL-MODY mice

To verify that the humanized *Cel* alleles were transcribed and translated into mature proteins, the expression of CEL-16R and CEL-MODY proteins were analysed in seven-week old heterozygous mice. Twelve mice were selected, six from each gender and four from each genotype. After sacrificing the mice, pancreata were isolated for preparation of pancreatic lysates. The protein concentration was measured for the lysates and 20 µg protein was loaded and separated by SDS-PAGE and analysed by western blotting.

The results are shown in Figure 5.2. In all samples, one band was detected just above 60 kDa, which is the expected size for wild-type mouse Cel protein (~66 kDa, Uniprot #Q64285). For CEL-16R mice, two additional bands were detected at 100 kDa and just below, suggesting humanized Cel with 16 VNTR repeats in a modified and unmodified state (El Jellas et al., 2018). As for the CEL-MODY mice, a band was detected just below 80 kDa, indicating a smaller Cel protein relative to the humanized 16R Cel, suggesting the truncated CEL-MODY protein. In the pancreatic lysates from female mice, one additional weak band was detected below 60 kDa, most likely due to unspecific antibody binding as seen in all female mice samples. Anti-beta actin was used as a loading control.

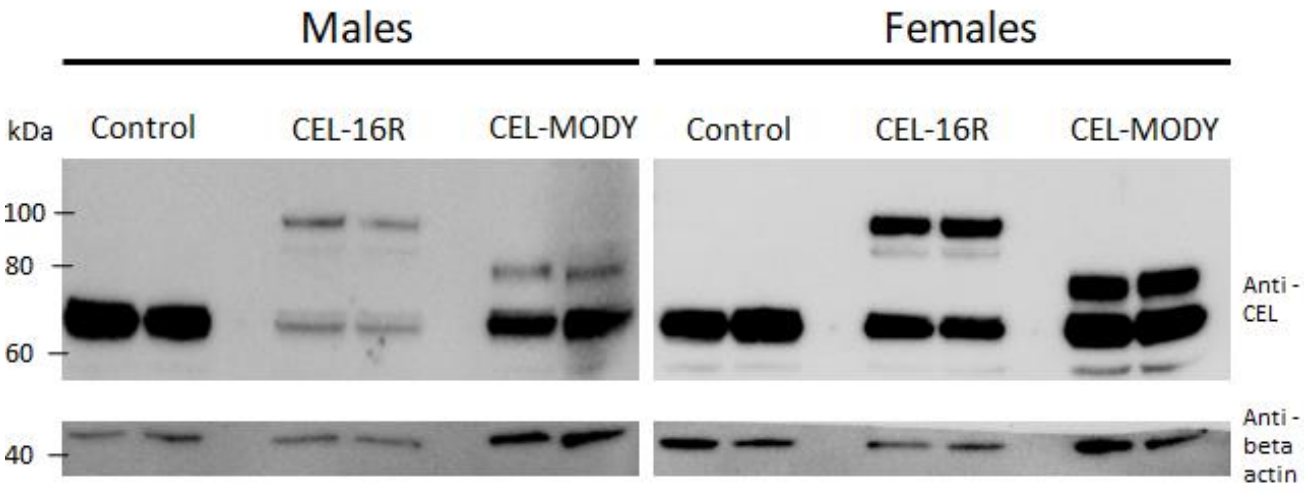

Figure 5.2. Expression of Cel protein variants in seven-week old mice. *Pancreatic lysates from controls and heterozygous CEL-16R and CEL-MODY mice were analysed by SDS-PAGE and western blotting. Cel expression was detected in both male and female mice by using an antibody targeting the globular domain of the Cel protein. Anti-beta actin was used as loading control.*

5.2 Mouse body weight development

All mice were weighed every other week to evaluate body weight development until the experimental end point at 3 or 6 months of age. For the mice with experimental end point at 6 months, both males and females followed a similar growth pattern for all three cohorts (Figure 5.3). However, male mice seemed to plateau after 24 weeks of age at around 34 g (Figure 5.3 A), whereas the female mice grew until the experimental end point, reaching a weight around 27-28 g (Figure 5.3 B). We found no statistically significant difference in body weight between the CEL-MODY, CEL-16R and control mice at 6 months. Male mice sacrificed at 3 months of age displayed a similar pattern (Appendix, Figure 1 A). However, female CEL-MODY and CEL-16R mice sacrificed at 3 months of age weighed significantly more than controls at experimental end point (Appendix, Figure 1 B). Large individual increases in body weight could be observed at certain ages. These increases later evened out with other mice during growth up to 14 weeks, indicating sporadic growth in certain mice. Furthermore, for all mouse strains, individual body weight seemed to vary within the strains, resulting in large error bars (*e.g.* standard error of the mean = ±1.624 g for CEL-MODY females at 6 months). This indicated that there were larger inter-individual variations rather than variations in the mean weight between the strains.

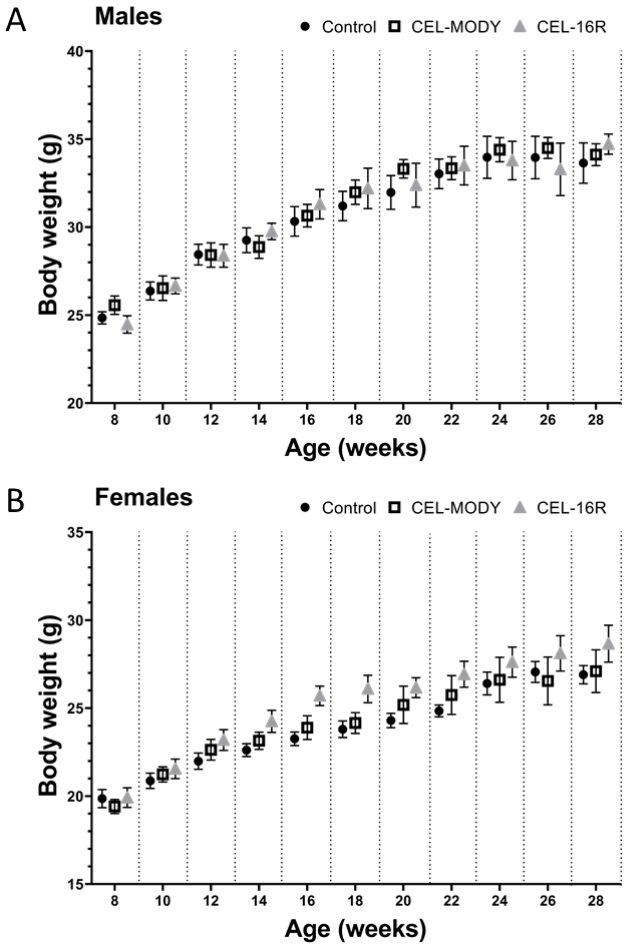

Figure 5.3. Body weight during life span of 6 months old CEL-MODY, CEL-16R and control mice. *The body weight (g) is presented as the mean at each age point for (A) males and (B) females. Error bars represent standard error of the mean. N=6-9.*

5.3 Weight of mouse pancreas

The pancreas weight of all mice was measured at the experimental end points (3 and 6 months) and plotted as percentage of body weight (Figure 5.4). For males at 3 months, the pancreas of the CEL-16R mice weighted significantly more compared to both controls ($P < 0.05$) and CEL-MODY ($P < 0.001$) mice (Figure 5.4 A). The same trend appeared after 6 months, however, the difference between CEL-16R and CEL-MODY were less prominent although still significantly different ($P < 0.05$). There were no significant differences in relative pancreas weight between the CEL-MODY and control mice.

For the females at 3 months of age, the relative pancreas weight of CEL-16R mice was also significantly higher compared to both controls ($P < 0.05$) and CEL MODY ($P < 0.01$) mice (Figure 5.4 B). This difference was not observed for the female mice at 6 months of age.

Taken together, the pancreas of the CEL-16R mice weighted significantly more compared to controls and CEL-MODY mice at 3 months, while less so or not significant at 6 months. Interestingly, the relative pancreas weight for female CEL-16R mice were higher at 3 months compared to the respective mice at 6 months.

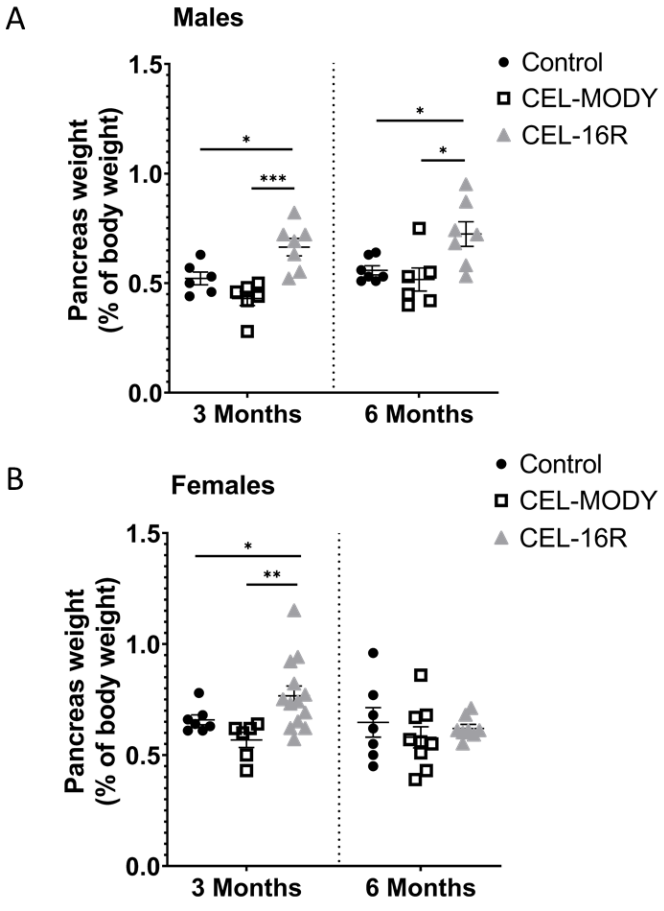

Figure 5.4. Pancreas weight of 3 and 6 months old CEL-MODY, CEL-16R and control mice. *The pancreas weight (expressed as percentage of body weight) of each mouse with mean (horizontal bar) are shown for each cohort at 3 and 6 months for (A) males and (B) females. Error bars represent standard error of the mean. Statistical significance is indicated as * ($P < 0.05$), ** ($P < 0.01$) and *** ($P < 0.001$). N=6-13.*

5.4 Pancreas histology of the CEL-MODY mice

To investigate if the CEL-MODY mice developed spontaneous chronic pancreatitis, we looked at the pancreas histology of 3 and 6 months old mice and compared them to CEL-16R and control mice. After sacrificing the animals, the pancreas was harvested and fixated for histological analysis. HE-stained sections for all the cohorts were evaluated. We included both male and female mice with n=6-9 in each cohort. For both control and CEL-16R mice, the pancreas showed normal lobular structures, and the morphology of both the exocrine and endocrine tissue appeared normal. However, several CEL-MODY mice showed signs of a pathological phenotype already at 3 months, which became more severe at 6 months for both genders. An overview of the number of CEL-MODY mice affected in each cohort is presented in Table 5.1.

Table 5.1. Overview of observed histological changes in the pancreas of CEL-MODY mice. *The pancreas phenotype was classified with no (normal), mild or severe pathological changes based upon the overall presence of pancreas atrophy and fat-infiltration, and their dominance over normal tissue in the pancreatic lobes.*

CEL-MODY cohort	Phenotype	n =
3 months, male	1 severely pathological, 2 mildly pathological, 3 normal	6
3 months, female	3 mildly pathological, 3 normal	6
6 months, male	4 severely pathological, 2 mildly pathological	6
6 months, female	6 severely pathological, 2 mildly pathological, 1 normal	9

HE-stained pancreas sections of selected male mice are presented in Figure 5.5 and Figure 5.6. At 3 months, one male CEL-MODY mouse showed signs of severe pathological phenotype in the pancreas (Figure 5.5). Here, we observed areas with major acinar tissue atrophy. Compared to control, we also found more intra- and interlobular fat.

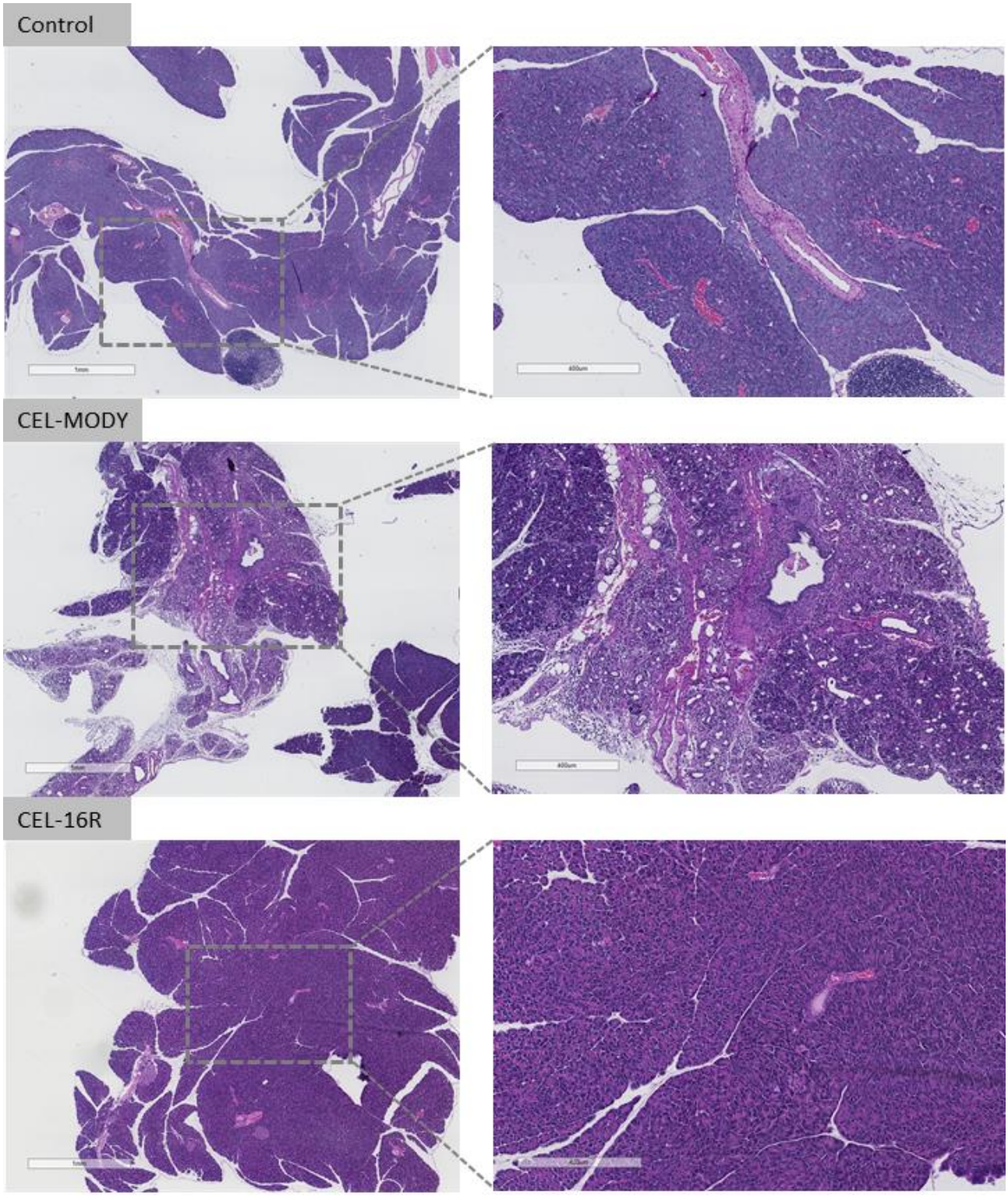

Figure 5.5. Pancreas histology of 3 months old CEL-MODY, CEL-16R and control mice. *HE-stained pancreatic sections of male mice. Note severe pancreas atrophy for the CEL-MODY mouse. Images with scale bars 1 mm (left panel) and 400 µm (right panel).*

At 6 months, all CEL-MODY mice, except one female mouse, showed a mild to strong pathological phenotype, driven by fat infiltration and acinar atrophy. In the pancreas of CEL-MODY mice, we

observed certain lobes that were heavily dominated by fat, whereas others appeared almost normal (Figure 5.6). Acinar atrophy was also observed, often surrounded by fat.

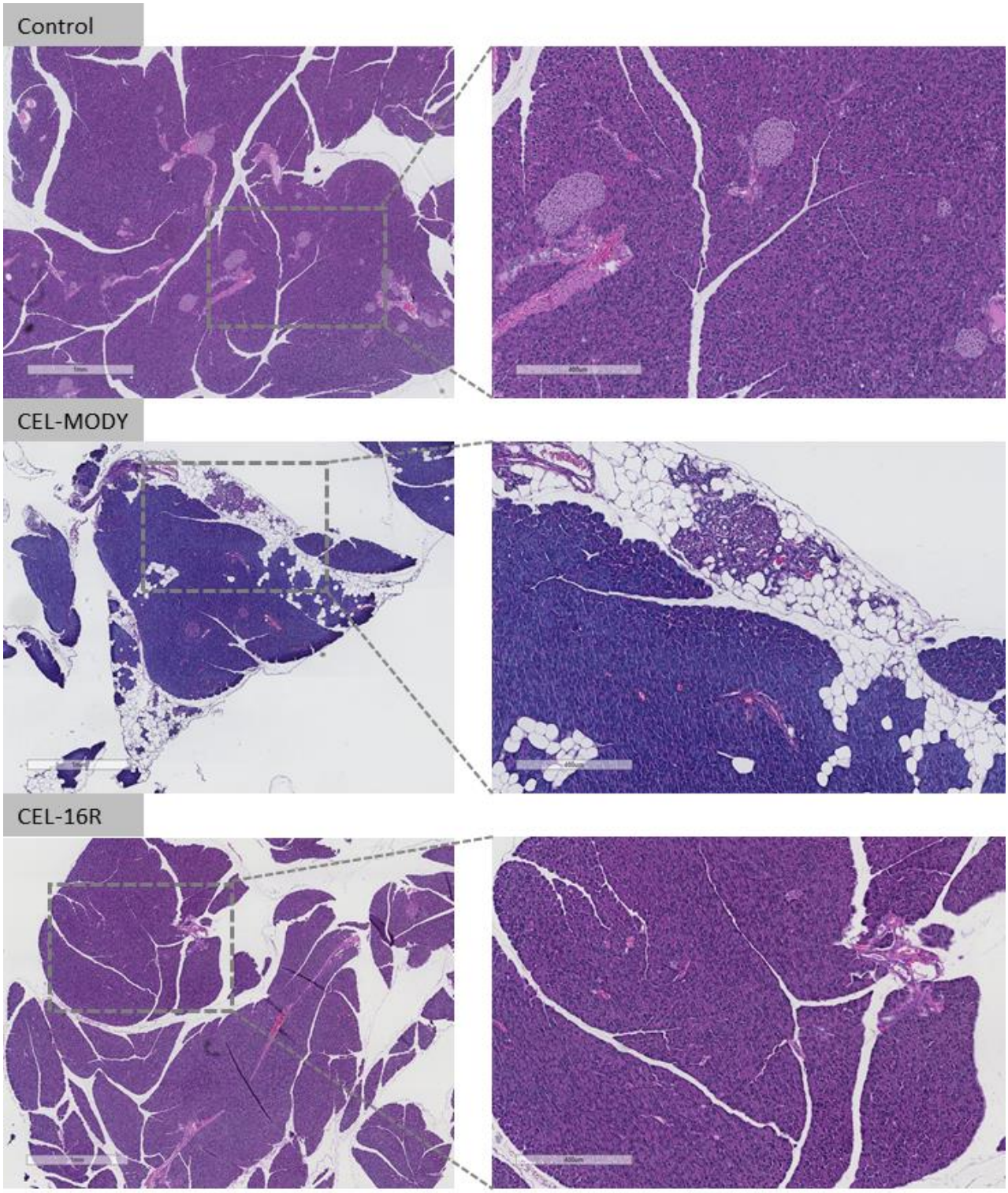

Figure 5.6. Pancreas histology of 6 months old CEL-MODY, CEL-16R and control mice. *HE-stained pancreatic sections of male mice. Note pancreas atrophy and fat infiltration for the CEL-MODY mouse. Images with scale bars 1 mm (left panel) and 400 µm (right panel).*

Taken together, some atrophy of acinar tissue was observed for the CEL-MODY mice already at 3 months of age, and was present in most mice at 6 months. There was fat-infiltration both between (inter) and within (intra) the lobes. At 6 months, this fat-infiltration seemed to dominate certain areas of the pancreas for most CEL-MODY mice, observed for both genders. The combination of fat infiltration and atrophy suggested that most CEL-MODY mice eventually would develop exocrine dysfunction.

5.5 Immunohistochemistry for Cel expression in the mouse pancreas

Pancreatic tissue sections from CEL-MODY, CEL-16R and control mice were analysed by immunohistochemistry for detection of both endogenous mouse Cel and CEL-MODY/CEL-16R proteins. For 3 months old CEL-16R and control mice, Cel staining was observed in the acinar cells of the exocrine pancreas (Figure 5.7). Upon closer inspection, Cel staining was observed in small grain-like structures in the apical part of acinar cells, indicating zymogen granules filled with Cel proteins. Positive Cel staining was also observed in some ducts confirming that Cel is secreted as part of the pancreatic juice. The endocrine islets were Cel negative. For the CEL-MODY mice, however, Cel was unevenly expressed in the exocrine tissue (Figure 5.7). More specifically, Cel expression seemed to be lost in several acinar cells. In addition, areas with a smeared pattern of Cel staining was observed, indicating the Cel proteins were no longer contained within the zymogen granules. The smeared pattern observed in CEL-MODY mice was found around acinar cells with no ducts present.

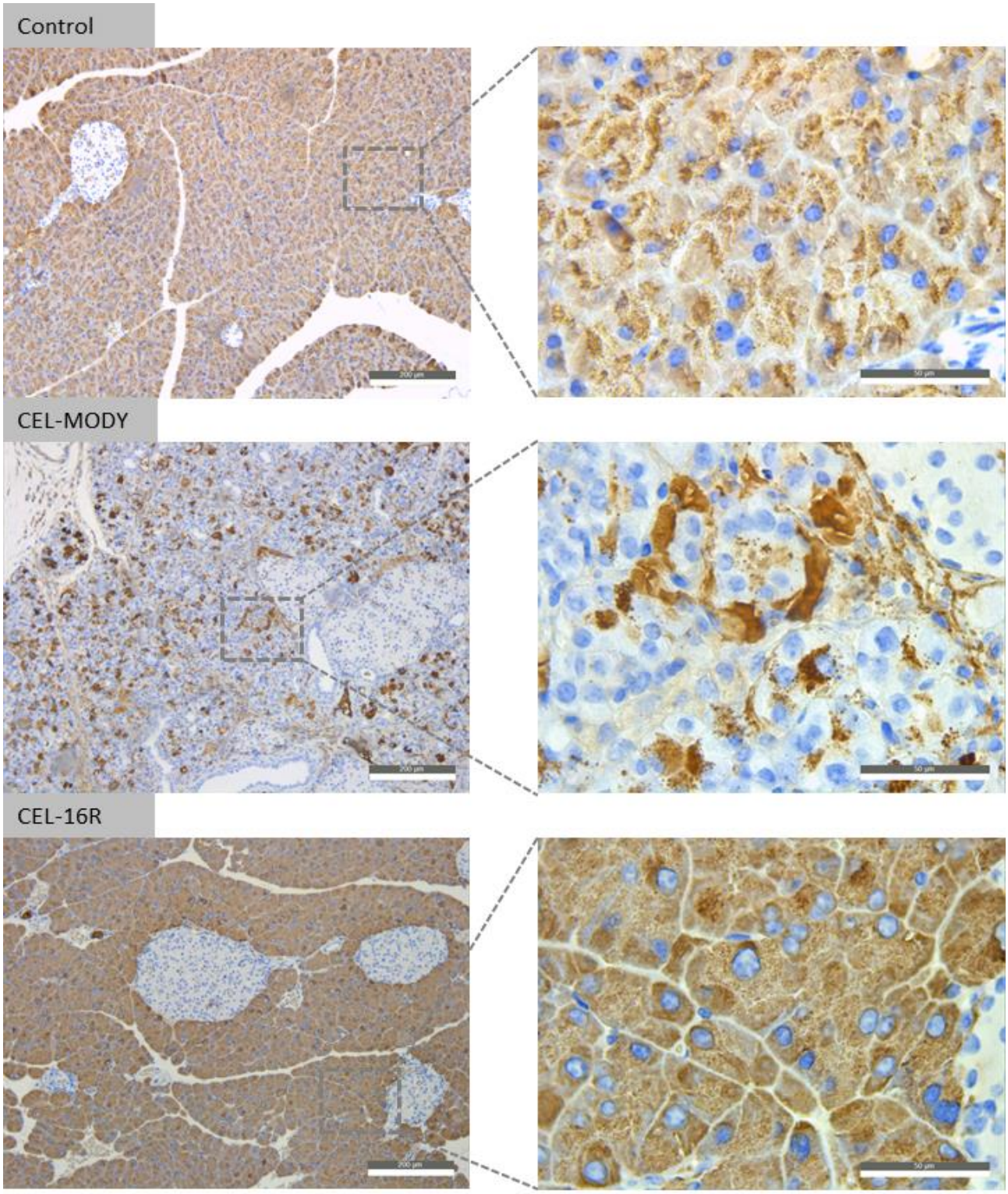

Figure 5.7. Immunohistochemistry for Cel expression in 3 months old CEL-MODY, CEL-16R and control mice. *Pancreatic sections from male mice were stained using an antibody targeting the globular domain of Cel. Note the uneven expression in CEL-MODY. Scale bars are 200 µm (left panel) and 50 µm (right panel).*

For the same CEL-MODY mouse, several areas with intensive Cel signals were observed as dark spots within the lumen of acini (Figure 5.8). These spots were observed in atrophic exocrine areas with low Cel expression and could suggest Cel protein aggregation.

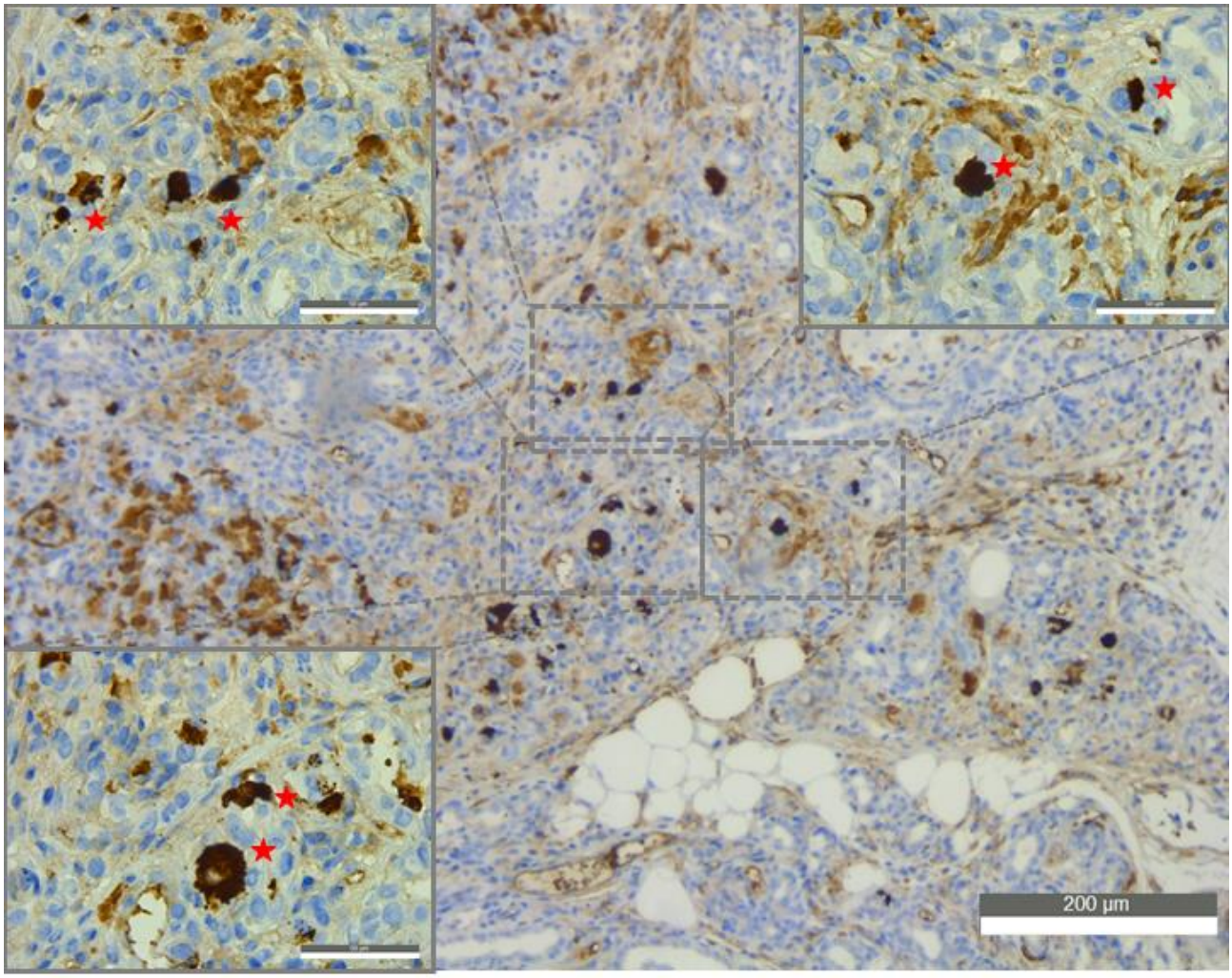

Figure 5.8. Potential Cel protein aggregates in CEL-MODY mice. *A pancreas section from one 3-month-old male CEL-MODY mouse was immunostained for detection of Cel expression. Red stars indicate areas of potential Cel protein aggregates. Scale bars are 200 µm and 50 µm.*

Compared to 3 months old mice, a similar Cel expression pattern was observed for CEL-16R and control mice at 6 months of age (Figure 5.9). In contrast, for the CEL-MODY mice at 6 months of age, certain lobes appeared to have normal Cel expression, while other lobes showed decreased Cel expression, indicating sporadic loss of Cel expression in the exocrine pancreas. The loss of Cel expression may further reflect the large morphological changes that we observed for the CEL-MODY mice.

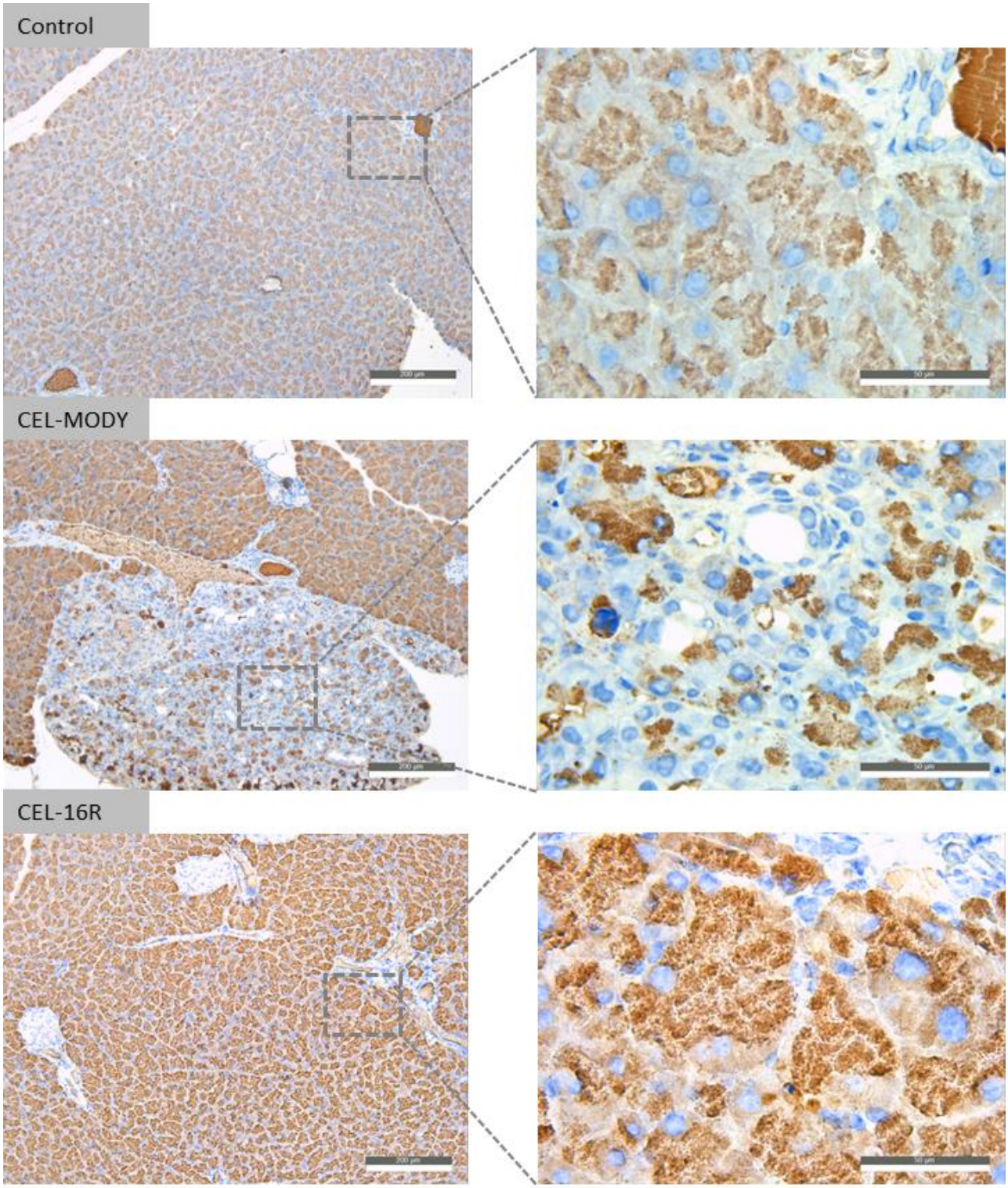

Figure 5.9. Immunohistochemistry for Cel expression in 6 months old CEL-MODY, CEL-16R and control mice. *Pancreatic sections from male mice were stained using an antibody targeting the globular domain of Cel. Note the uneven expression in one lobe in the CEL-MODY mouse. Scale bars are 200 µm (left panel) and 50 µm (right panel).*

As described in section 5.4, fat infiltration of the pancreas became prominent at 6 months of age for most CEL-MODY mice. When performing immunostaining, we observed Cel positive staining between fat cells that most likely had replaced the acinar tissue (Figure 5.10). Upon closer inspection

of these areas, low intensity Cel staining was observed close to the nucleus of some fat cells, suggesting a previous presence of Cel expressing acinar cells.

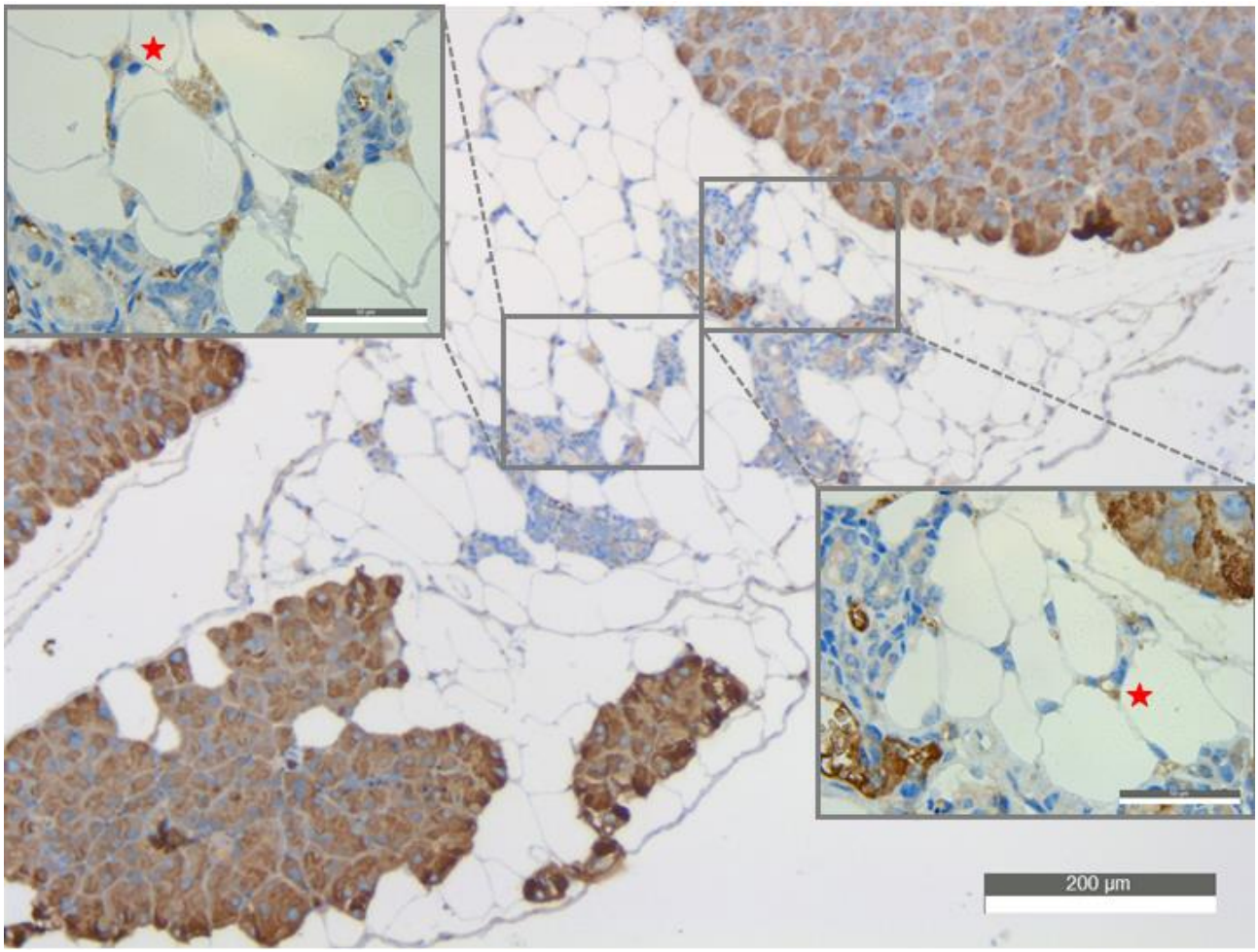

Figure 5.10. Identification of Cel proteins between infiltrating fat cells. *A pancreas section from one 6-month-old male CEL-MODY mouse was immunostained for detection of Cel expression. Red stars indicate areas of Cel positive staining between fat cells. Scale bars are 200 µm and 50 µm.*

5.6 Staining for fibrotic tissue in CEL-MODY mice

Pancreatic fibrosis is a characteristic feature of CP. To investigate if the CEL-MODY mice had signs of fibrosis development, we performed trichrome staining on pancreatic sections from 3 and 6 months old male mice. CEL-16R and control mice were included in the experiment and the results are presented in Figures 5.11 and 5.12. With the Ventana trichrome staining procedure, collagen (and consequently connective tissue) is stained in blue, cytoplasm in red while hematoxylin stains the nucleus violet. Collagen is a protein which is overrepresented in fibrotic tissue. In a normal pancreas, ducts and blood vessels are surrounded by connective tissue, as evident in the CEL-16R and control mice (Figure 5.11 and Figure 5.12). For the CEL-MODY mice, however, we observed large areas of

pancreatic tissue that had severe scarring, indicated by wide-spread fibrosis. In some areas, hardly any normal exocrine tissue was left (Figure 5.11 and Figure 5.12).

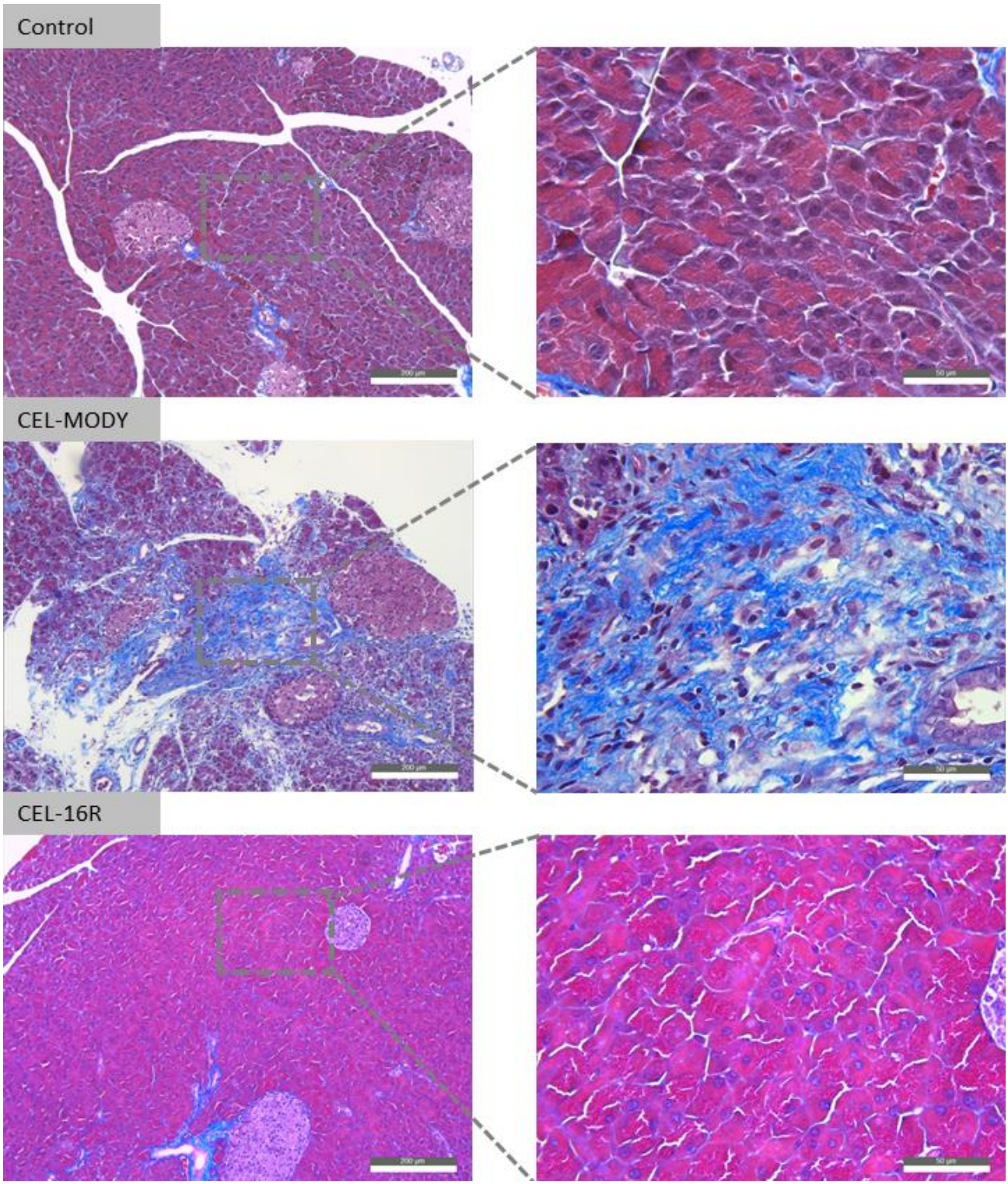

Figure 5.11. Trichrome staining of pancreatic tissues in 3 months old CEL-MODY, CEL-16R and control mice. *Pancreas sections from male mice were stained. Connective tissue is stained blue. Note the widespread fibrosis in CEL-MODY. Scale bars are 200 µm (left panel) and 50 µm (right panel).*

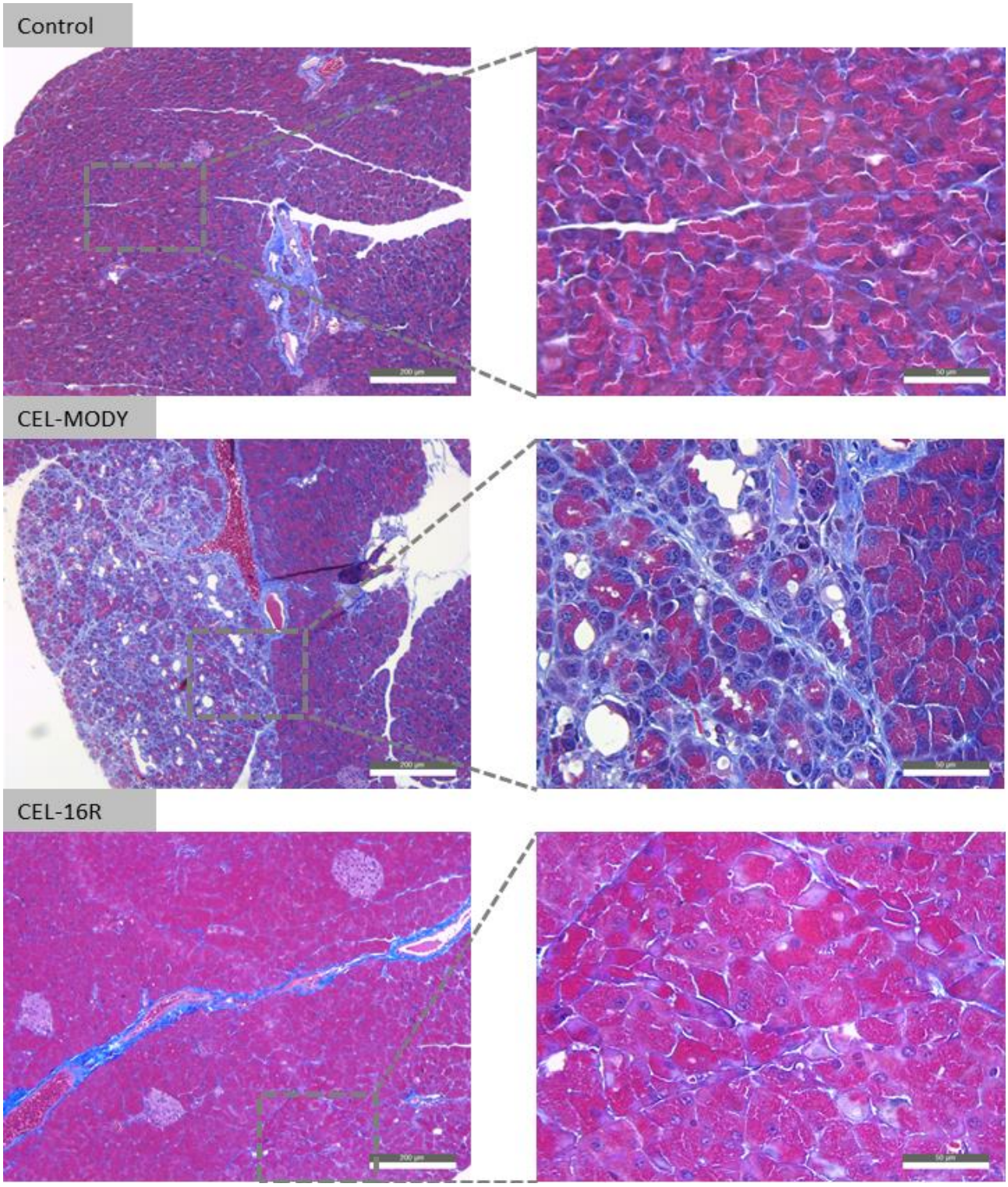

Figure 5.12. Trichrome staining of pancreatic tissues in 6 months old CEL-MODY, CEL-16R and control mice. *Pancreas sections from male mice were stained. Connective tissue is stained blue. Note the widespread fibrosis in CEL-MODY. Scale bars are 200 µm (left panel) and 50 µm (right panel).*

When further analysing the CEL-MODY mice, we observed several small duct-like structures in areas with wide-spread fibrosis (Figure 5.13). These could be distinguished from normal ducts by being small in size and the absence of pancreatic juice. They also appeared in a large quantity, in areas with almost no normal acinar tissue. Furthermore, some of these duct-like structures appeared to fuse with

each other, increasing their size. The presence of these duct-like structures may suggest acinar-to-ductal metaplasia (ADM).

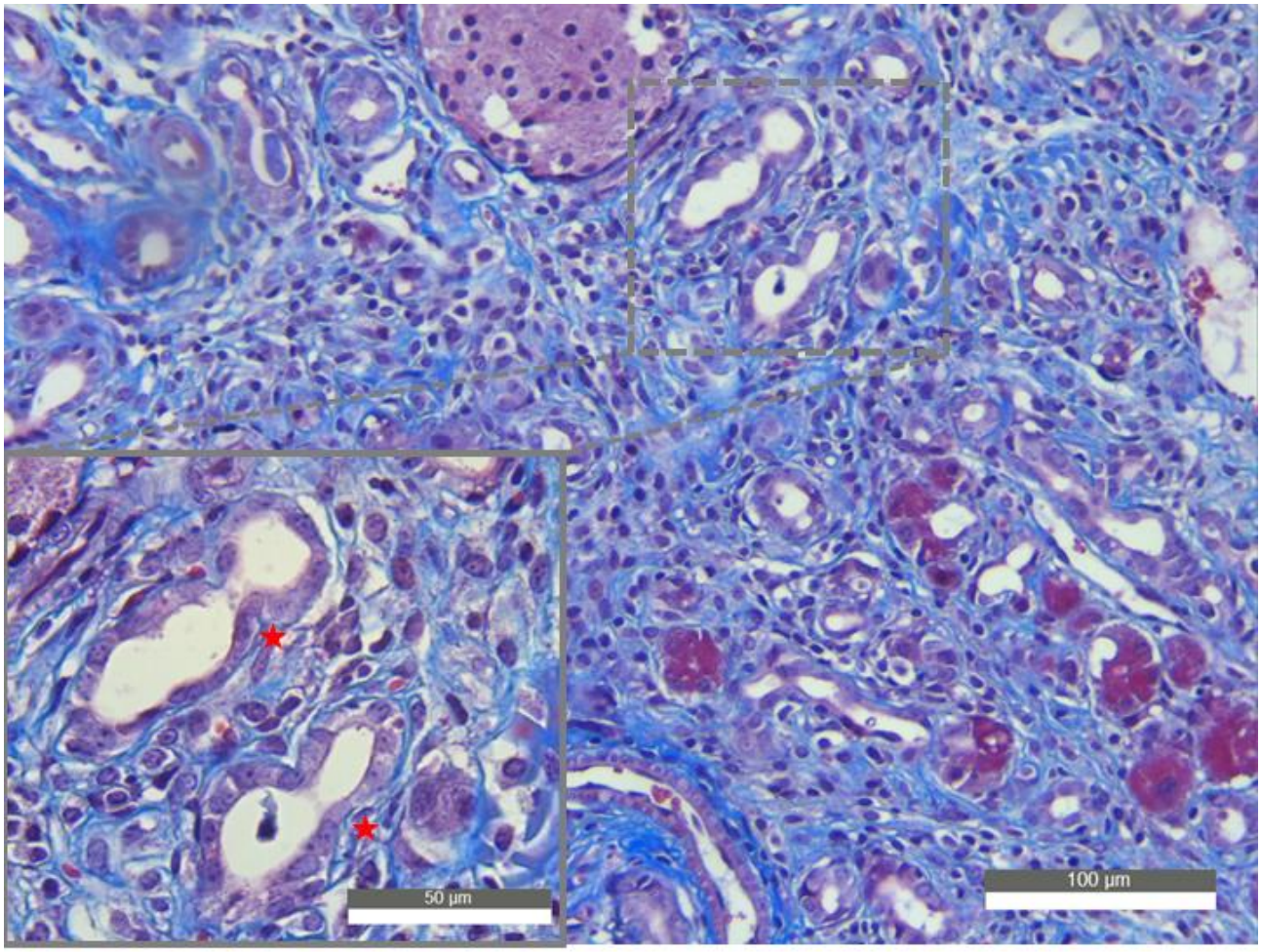

Figure 5.13. Potential acinar-to-ductal metaplasia detected in CEL-MODY mice. *Pancreas section from one 3-month-old male CEL-MODY mouse was stained with trichrome for detection of fibrosis. Red stars indicate fusing duct-like structures. Scale bars are 100 µm and 50 µm.*

Interestingly, when analysing the CEL-MODY mice for pancreas histology, most endocrine tissue seemed unaffected despite the damage to the exocrine tissue surrounding it. Also, when analysing CEL-MODY mice by trichrome staining, we observed intact islets surrounded by fat. However, some of these islets were observed in closer proximity to each other compared to what was observed in normal pancreatic tissue (Figure 5.14). In addition, in some CEL-MODY mice, the endocrine islets were somewhat enlarged (Figure 5.7), which could suggest islet fusion.

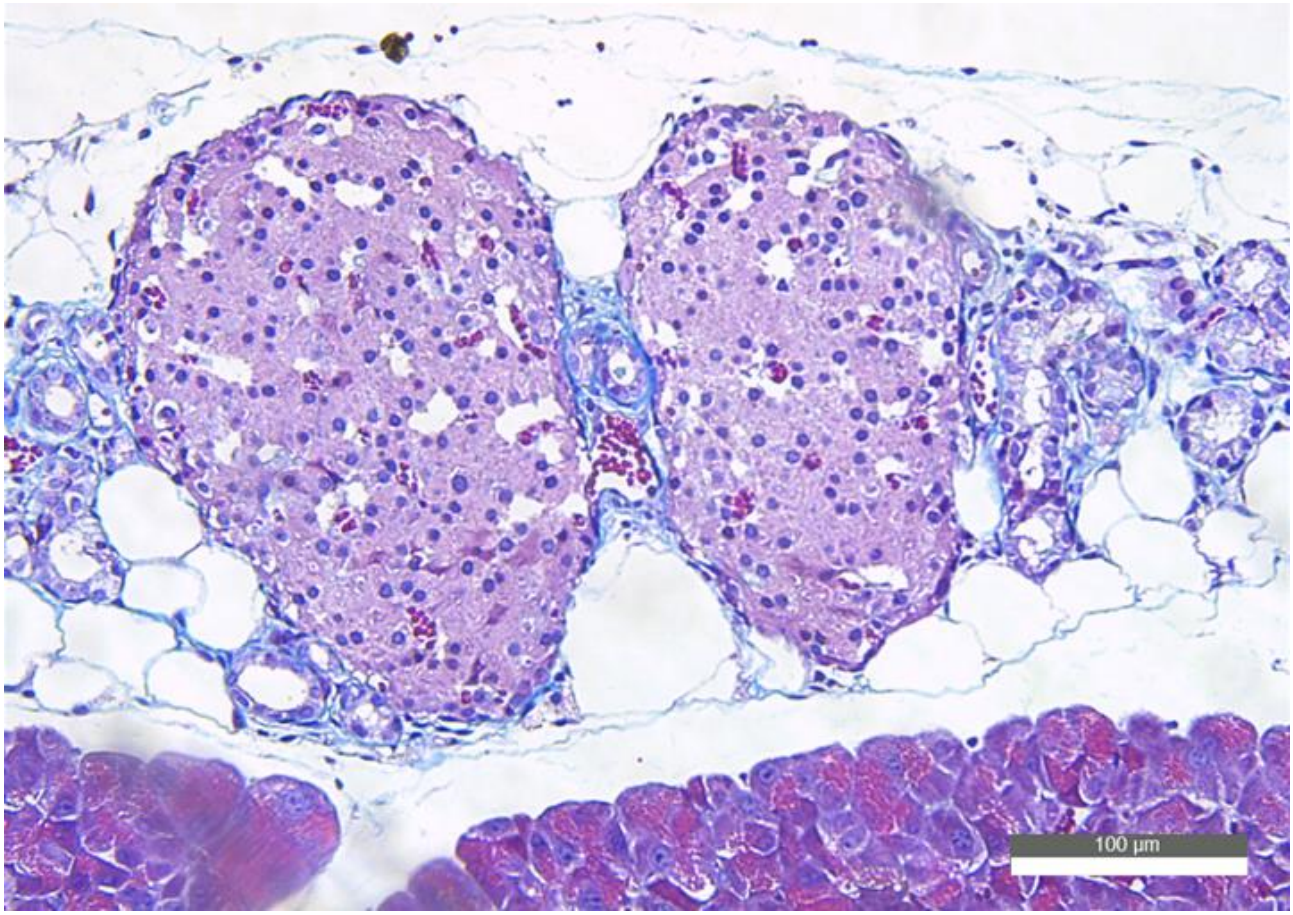

Figure 5.14. Pancreatic islets surrounded by fat and fibrosis in CEL-MODY mice*. Pancreas section from one 6-month-old male CEL-MODY mouse was stained with trichrome for detection of fibrosis. Note the two narrow islets being surrounded by fat and fibrotic tissue. Scale bar is 100 µm.*

5.7 Glucose homeostasis tests in mice

To investigate if the CEL-MODY mice were diabetic, we measurred their abilty to regulate blood glucose by performing an IPGTT. At 6 month of age, no differences were observed between CEL-MODY, CEL-16R and control mice, for either males or females, indicating normal glucose tolerance (Figure 5.15). Mice at 3 months of age showed the same pattern (Appendix, Figure 2).

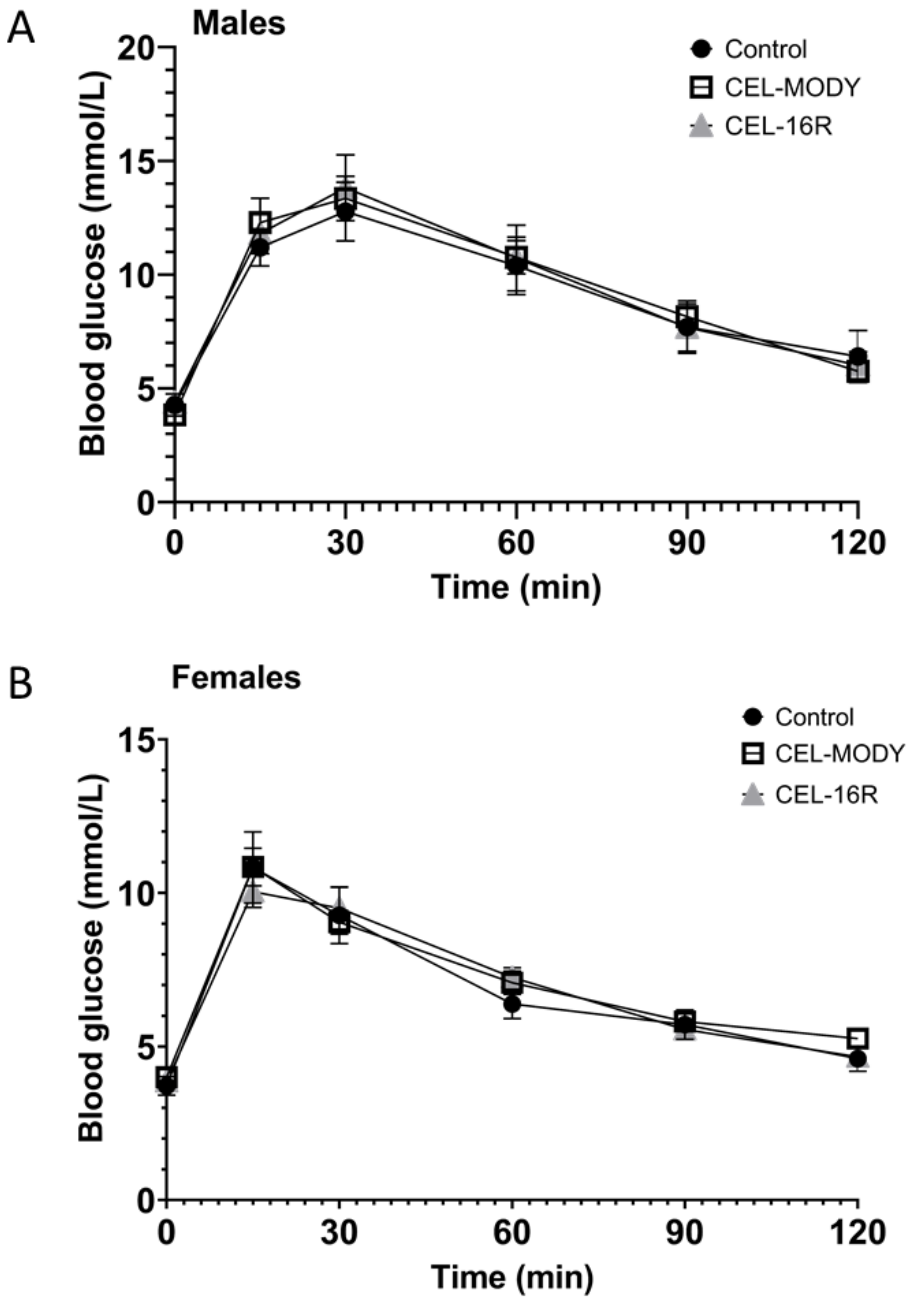

Figure 5.15. Intraperitoneal glucose tolerance test for 6 months old mice. *Time 0 represents blood glucose measurments before injection. CEL-MODY, CEL-16R and control mice are compared for (A) males and (B) females and represented by the mean for each strain. Error bars represent standard error of the mean.*

Furthermore, we also performed an IPITT for mice at 6 months of age (Figure 5.16). No statistical difference could be observed in insulin sensitivity between CEL-MODY and control mice, indicating normal insulin sensitivity. However, 60 minutes after insulin injection, the CEL-16R male mice showed a statistically significant increase ($P < 0.05$) in blood glucose compared to both CEL-MODY and control mice (Figure 5.16 A). Then, 90 and 120 minutes after injection, the CEL-16R mice were still significantly higher than the control mice ($P < 0.01$) but not higher than the CEL-MODY mice. For the CEL-16R female mice, similar pattern was observed (Figure 5.16 B).

When performing the IPITT on mice 3 months old mice, the blood glucose dropped too low, including some that went into a hypoglycemic shock. The mice were all saved by glucose injections, however, they were excluded from the study.

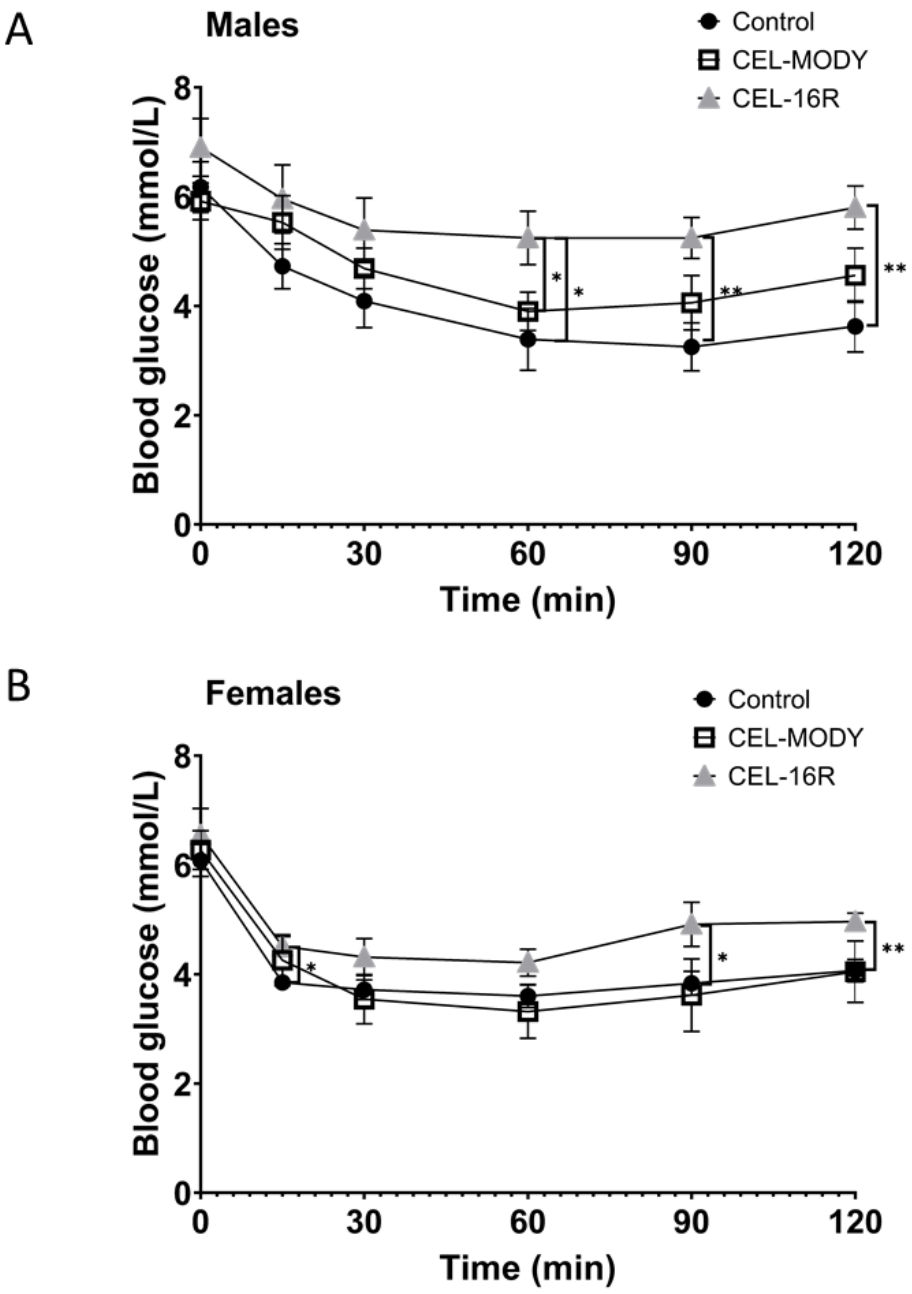

Figure 5.16. Intraperitoneal insulin tolerance test for 6 months old mice. *Time 0 represents blood glucose measurments before injection. CEL-MODY, CEL-16R and control mice are compared for (A) males and (B) females and represented by the mean for each strain. Error bar represents standard error of the mean.*

6 Discussion

In 2006, our research group was the first to describe the pathogenic mutations in *CEL* known as CEL-MODY. Since then, both cellular and clinical studies have been performed to learn more about the underlying disease mechanisms. Currently, we believe that CEL-MODY is a protein misfolding disease. Cellular studies have shown that the human CEL-MODY protein forms both intra- and extracellular aggregates that causes proteotoxic damage, ER-stress and apoptosis (Johansson et al., 2011, Torsvik et al., 2014, Xiao et al., 2016). Clinically, the CEL-MODY syndrome is characterized by early exocrine dysfunction, followed by diabetes (Ræder et al., 2006). However, patients with the CEL-MODY syndrome also fulfil the criteria for CP (M. Lowe, pers. comm). Actually, two new CEL-MODY families from the Czech Republic and Sweden developed signs of CP before the manifestation of endocrine insufficiency occurred (Unpublished; A. Molven, pers. comm). Thus, CEL-MODY might as well be regarded as a form of inherited CP rather than a monogenic form of diabetes.

In this study, we aimed to take our CEL-MODY research to the next level: we wanted to investigate the effect of CEL-MODY protein aggregation at the organ level. This was done by characterizing the phenotype of a newly developed CEL-MODY mouse strain. We evaluated whether the mouse strain was able to recapitulate the human phenotype observed in persons carrying the *CEL-MODY* mutation by investigating both male and female mice at 3 and 6 months of age, using both the CEL-16R strain and wild-type mice as controls.

6.1 The first mutant lipase mouse model for CP

The search for genetic variants associated with CP has been extensive since the first *PRSS1* mutation was discovered in 1996 (Whitcomb et al., 1996). For many years, most of the genetic variants characterized were linked to the trypsin-dependent pathway (Hegyi and Sahin-Tóth, 2017). Consequently, the trypsin-dependent pathway has dominated our way of thinking about the disease and mouse models have been constructed to understand the role of trypsin in CP (Geisz and Sahin-Tóth, 2018, Troy and Maxim, 2018).

In this master project, however, we describe the first mutant lipase mouse model for CP development. Interestingly, heterozygous CEL-MODY mice at both 3 and 6 months showed typical hallmarks for CP including pancreatic atrophy, fibrosis, potential ADMs and fatty-infiltration. Based on cellular studies by us and others (Johansson et al., 2011, Torsvik et al., 2014, Xiao et al., 2016) and the fact that we observed signs of Cel protein aggregates in the pancreas of CEL-MODY mice, we believe

that CEL-MODY is acting through the alternative misfolding-dependent pathway (Sahin-Toth, 2017). Similarly, Hegyi and Sahin-Tóth have shown that a human *CPA1* mutation also results in protein misfolding and ER-stress in both cellular and mouse models (Hegyi and Sahin-Tóth, 2019). Furthermore, the *CPA1* mutant mice developed progressive acinar cell atrophy, inflammation, fibrosis and ADM. These findings correlate well with what we observed for the CEL-MODY mouse. However, additional analyses are needed to confirm induced ER-stress as well as inflammation in our CEL-MODY model.

6.2 The CEL-MODY mouse recapitulates many of the features of CEL-MODY patients

When the two Norwegian CEL-MODY families were identified, they presented symptoms of low fecal elastase, steatorrhea and fatty infiltration, indicating exocrine dysfunction (Ræder et al., 2006, 2007). In a follow-up study on these patients, reduced digestive enzyme levels and bicarbonate in the pancreatic juice was detected, confirming reduced exocrine function (Tjora et al., 2013). Unfortunately, we did not have the time to measure pancreatic exocrine function in our mice (see section 6.7). However, we observed reduced Cel expression in atrophic exocrine tissue of CEL-MODY mice, suggesting that the degradation of the exocrine tissue reduces the overall expression of digestive enzymes during CP development. Interestingly, the relative pancreas weight of CEL-MODY mice did not decrease significantly compared to control mice as one could expect with massive exocrine atrophy. However, the fatty infiltration may be compensating for the loss of acinar cells and thereby keeping the overall weight stable.

Fatty infiltration of the pancreas was a prominent feature in the CEL-MODY mice. Even so, these mice were not obese (no statistical significance compared to controls), excluding that overweight was a contributing factor. This correlates with similar observations for CEL-MODY patients as they were not overweight and had fatty infiltration of the pancreas, also in young non-diabetic subjects (Ræder et al., 2007). For the patients, the fatty pancreas was speculated to play a role in diabetes development, which usually occurred in their 40s. We did not detect any signs of diabetes development in the CEL-MODY mice. Even when there was hardly any exocrine tissue left, the islets were still present and somewhat enlarged in size. Similar observations were seen in a mouse model for CP driven by trypsinogen activation, where fatty infiltration became dominant in later stages of CP, but no endocrine dysfunction was detected (Geisz and Sahin-Tóth, 2018). For the CEL-MODY mice, prolonging the experimental end point to 9 or 12 months might be sufficient for diabetes to manifest. Alternatively, a high-fat diet (HFD) can be used for Black-6 mice to induce metabolic diseases

(Fisher-Wellman et al., 2016). Actually, symptoms of impaired glucose tolerance have been observed in these mice after only 1-3 days into HFD (Fisher-Wellman et al., 2016). Therefore, putting the CEL-MODY mice on an HFD would be interesting - whether that would trigger diabetes development.

6.3 Fat infiltration of the pancreas

In human adults, fat infiltration of the pancreas is common and mostly considered a benign condition (Coulier, 2016). Age and visceral fat index correlate to the grade of fatty infiltration. In extreme cases, fat infiltration may lead to exocrine pancreatic dysfunction and is found associated with diseases such as diabetes, pancreatitis, cystic fibrosis and other metabolic syndromes (Coulier, 2016). The precise etiology is often indecisive although fatty infiltration is regularly observed as secondary phenotype in disease progression.

As mentioned previously, fatty infiltration is part of the phenotype of pancreatitis patients, including CEL-MODY patients (Ræder et al., 2007, Majumder et al., 2017). Interestingly, we observed severe fatty infiltration of the pancreas in 6 months old male and female CEL-MODY mice. The fat content seemed to increase with age as the phenotype was less prominent in the 3 months old mice. However, the origin of these fat cells remains a mystery.

One hypothesis is that the fat cells are recruited from the peripancreatic fat tissue. Another hypothesis could be transdifferentiation, that acinar cells have differentiated into adipose cells. Acinar cells are prone to differentiation by cellular reprogramming, as beta-cell regeneration from acinar cells are used in diabetes therapy research (Kim and Lee, 2016). Furthermore, inactivation of the transcription factor *c-myc* have shown to cause loss of acinar maturation, leading to decreased pancreas mass and transdifferentiation into adipocytes (Bonal et al., 2009). ADM is another differentiation process driven by growth factors (Liu et al., 2016) and is arguably seen in the CEL-MODY mouse (Figure 5.13). Interestingly, we observed positive Cel staining between adipocytes in the CEL-MODY pancreas (Figure 5.10), which may suggest that transdifferentiation from acinar cells has occurred. However, it is not clear whether the staining is present within or outside these adipocytes. Further experiments (*e.g.* electron microscopy) should be done to differentiate whether the Cel proteins are within the adipocytes or Cel protein are diffusing between the adipocytes from acinar leakage of zymogen granules. Actually, our research group is planning to follow up on this and do cell lineage tracing in CEL-MODY mice, to identify the origin of these infiltrating adipocytes.

6.4 Cel expression during CP development in mice

Together with other digestive enzymes, Cel is secreted from the apical part of acinar cells as part of the zymogen granules. In control mice, we observed normal Cel expression throughout the exocrine pancreas, and when inspected closely, small grain-like structures were observed indicating the zymogen granules (Figure 5.7 and 5.9). These zymogen granules were seen polarized from the nucleus of the acinar cells, indicating normal secreting acinar cells (El Jellas et al., 2018). In CEL-MODY mice, certain pancreatic areas showed reduced Cel expression as the exocrine tissue became more atrophic. A similar pattern is seen in pancreatic cancer where CEL expression is lost during ADM (El Jellas et al., 2018). Although abnormal exocrine tissue and Cel expression were seen in the CEL-MODY mice, some areas were normal, similar to control mice, indicating sporadic origin of pathogenesis in the CEL-MODY pancreas.

Furthermore, we observed some patchy staining in the CEL-MODY mouse that could potentially indicate protein aggregation (Figure 5.8). However, it is not possible to determine if these proteins are present within the acinar cells or secreted into the acinus lumen. Previous cell culture studies have shown that the CEL-MODY protein form insoluble oligomers in both lysate and pellet fractions when analysed by western blotting, and protein aggregates were observed both intra- and extracellularly when analysed by electron microscopy and immunofluorescence (Johansson et al., 2011, Torsvik et al., 2014). Thus, we believe that these CEL-MODY aggregates also are present in the CEL-MODY mice and that they are the origin of pathogenesis for CP development. However, further investigation (*e.g.* electron microscopy) of the CEL-MODY mouse pancreas will provide more insight into the presence and location of these protein aggregates.

6.5 Disease progression in CEL-MODY mice

In secretory cells, protein misfolding in the ER activates the unfolded protein response (UPR) in an attempt to maintain cell viability and function (Hetz, 2012). CEL-MODY protein misfolding has also shown to activate the UPR in cellular studies (Xiao et al., 2016). Consequentially, UPR induced ER-stress with elevated expression of the binding immunoglobulin protein (BiP) and X-box binding protein 1 (XBP1) (Xiao et al., 2016). In addition, the human *CPA1* mutation mouse model discussed in section 6.1 showed induced ER-stress detected by markers such as the C/EBP homologous protein (CHOP) and BiP (Hegyi and Sahin-Tóth, 2019). Induced ER-stress by protein misfolding is one of the hallmarks in genetic CP for digestive enzymes following the misfolding-dependent pathway (Sahin-Toth, 2017, Mayerle et al., 2019).

Irreversible ER-stress trigger cell death by apoptosis, which has shown to be activated by nuclear factor kappa-light-chain-enhancer of activated B-cells (NF-κB) in cellular studies on CEL-MODY (Xiao et al., 2016). There is a crosstalk between UPR induced ER-stress markers and NF-κB that links protein misfolding to apoptosis (Schmitz et al., 2018). Furthermore, the activation of NF-κB in acinar cells are thought to induce inflammation by production of inflammatory cytokines (Murtaugh and Keefe, 2015). These cytokines stimulate activation of macrophages, which we unfortunately did not have time to investigate in the CEL-MODY mouse pancreas (discussed in section 6.7). Notably, inflammation was observed for the human *CPA1* mutated mouse model by immunohistochemistry for the membrane protein F4/80 on macrophages (Hegyi and Sahin-Tóth, 2019).

Within the exocrine pancreas lies quiescent pancreatic stellate cells (PSCs), which are activated upon inflammation and starts producing extracellular matrix (ECM) proteins, promoting fibrosis (Hamada et al., 2015). One of these ECM proteins is type 1 collagen, which we stained for in the CEL-MODY mice. We observed long fibre-like structures indicating fibrosis development, which is one of the main hallmarks of CP (Etemad and Whitcomb, 2001, Hegyi and Sahin-Tóth, 2019).

In addition to ECM proteins, PSCs secrete growth factors such as TGF-beta (Xue et al., 2018), known to initiate dedifferentiation in acinar cells to ductal-like cells (Liu et al., 2016). We observed tubular duct-like structures within fibrotic areas in the CEL-MODY mouse, suggesting that activated PSCs in these areas both induced fibrosis and ADM. However, immunostaining for specific ADM markers such as sox9 and cytokeratin 19 would give more compelling evidence (Hessmann et al., 2016, Hegyi and Sahin-Tóth, 2019).

Human chronic pancreatitis often leads to extensive fibrosis. However, in a mouse model for trypsin associated CP, they observed early CP with dilated ducts and fibrosis before fatty infiltration dominated in late stage CP (Geisz and Sahin-Tóth, 2018). This disease progression might be similar to what happens in the CEL-MODY mouse, although CEL-MODY follows a trypsin-independent pathway.

Based upon current literature and the results in this study, we suggest that the pathological progression in the CEL-MODY mouse starts by misfolding of the CEL-MODY protein. This leads to formation of protein aggregates that induce ER-stress, apoptosis and inflammation. Further, inflammation activates PSCs which induces fibrosis and ADM before fatty infiltration takes over in later stage of disease. Nevertheless, additional studies are needed to make a precise progression model. It is noteworthy to mention the sporadic pathological development observed when investigating the pancreas of the CEL-MODY mouse. The morphological changes do not happen uniformly throughout

the pancreas, as certain lobes seem to be more affected than others. Interestingly though, this is commonly seen in patients with CP as well (C. Verbeke, pers. comm).

The presence of potential ADM in the CEL-MODY mouse is also interesting in terms of pancreatic cancer development. Invasive PDAC do mostly origin from ADM accumulating pre-invasive precursor lesions (Liu et al., 2016). As mentioned in the introduction part of this thesis (section 1.5.1), PDAC has been observed in one older member of a CEL-MODY family. Interestingly, over 90 % of all PDAC cases harbour a mutation in the oncogene *KRAS* (Orth et al., 2019). However, a *KRAS* mutation alone is not enough to trigger development of invasive PDAC (Liu et al., 2016). Crossbreeding the CEL-MODY mouse with a *KRAS* mouse strain would therefore be very interesting in order to investigate if the CEL-MODY protein aggregates could trigger invasive pancreatic cancer in *KRAS* mouse.

6.6 The CEL-16R mouse

Compared to human *CEL*, the mouse *Cel* gene harbour only three VNTR repeats and the amino acid composition differ from the human VNTR (Holmes and Cox, 2011). Therefore, a CEL-16R mouse model was designed as a control to exclude the possibility that the human *CEL* VNTR *per se* could cause any pathological phenotype in the mouse. Similar to the wild-type controls, no morphological changes were observed in the pancreas of the CEL-16R mice, suggesting that the mice were healthy. However, the relative pancreas weight of the CEL-16R mice were significantly higher than for both wild-type controls and CEL-MODY mice, with the exception of females at 6 months of age (Figure 5.4). In addition, the CEL-16R mice showed decreased insulin sensitivity compared to both wild-type controls and CEL-MODY mice (Figure 5.16). Taken together, we observed some differences between the CEL-16R mice and the wild-type control mice. Thus, we need to characterize the CEL-16R mice in more detail to be more confident about their phenotype, and to decide if they can be used as true controls or not.

6.7 The impact of Covid-19 on the master project

Due to the Covid-19 global health crises, strict guidelines were provided by the Norwegian Government. This involved a temporary lockdown of all laboratory work at the University of Bergen and Haukeland University Hospital. The lockdown lasted 6 weeks and therefore, two experiments planned for this thesis, were discarded due to lack of time. One of these experiments was immunohistochemistry for F4/80, a marker for inflammation. The other experiment was to analyse

serum alpha amylase activity, which is a way of measuring pancreatic exocrine function (Madole et al., 2016). Upon pancreas damage and CP, there is leakage of digestive enzymes into the blood stream and elevated levels of amylase in serum indicate pancreatic exocrine dysfunction.

7 Conclusion

The CEL-MODY syndrome is characterized by early exocrine dysfunction and diabetes. Although the syndrome was discovered as a monogenic form of diabetes, new insight might suggest that the diabetes develops secondary to exocrine dysfunction and CP. Here, the overall objective was to investigate the phenotype of a new transgenic CEL-MODY mouse strain – to see whether mice and human develop the same characteristic features and to learn more about the underlying mechanisms.

We found that the CEL-MODY mouse developed acinar cell atrophy, fibrosis, potential ADM and fatty infiltration in the pancreas already at 3 months of age. These are well-known signs of CP - which became more severe at 6 months of age for both male and female CEL-MODY mice. We also observed potential Cel protein aggregates in the CEL-MODY pancreas, supporting that the mice develops disease through the misfolding-dependent pathway of CP. At 6 months of age, we did not observe any diabetes development in this model.

8 Future perspectives

With the CEL-MODY mice, we have developed a new animal model for CP. This gives us a range of possibilities for follow-up studies. However, to finish the first characterization study of the mice, we will focus on the experiments listed below.

Perform

- immunohistochemistry for the F4/80 marker in the pancreas of CEL-MODY mice to analyse the presence of inflammation
- measure pancreatic alpha-amylase activity from blood serum collected from CEL-MODY mice to analyse pancreatic exocrine dysfunction
- investigate up-regulation of ER-stress markers in acinar cells of CEL-MODY mice by western blotting
- investigate the presence and location of protein aggregates in CEL-MODY mice by electron microscopy
- perform immunohistochemistry for specific ADM markers in the pancreas to confirm its presence in CEL-MODY mice.
- extend the experimental end point for CEL-MODY mice to 9- and 12 months to investigate whether they develop diabetes by IPGTT and IPITT
- feed the CEL-MODY mice with an HFD to push them into glucose intolerance and to investigate if they develop diabetes by IPGTT and IPITT

References

ABOUAKIL, N. & LOMBARDO, D. 1989. Inhibition of human milk bile-salt-dependent lipase by boronic acids. Implication to the bile salts activator effect. *Biochim Biophys Acta,* 1004**,** 215-20.

ABOUAKIL, N., MAS, E., BRUNEAU, N., BENAJIBA, A. & LOMBARDO, D. 1993. Bile salt-dependent lipase biosynthesis in rat pancreatic AR 4-2 J cells. Essential requirement of N-linked oligosaccharide for secretion and expression of a fully active enzyme. *J Biol Chem,* 268**,** 25755-63.

AFROZE, S., MENG, F., JENSEN, K., MCDANIEL, K., RAHAL, K., ONORI, P., GAUDIO, E., ALPINI, G. & GLASER, S. S. 2013. The physiological roles of secretin and its receptor. *Annals of translational medicine,* 1**,** 29-29.

AMERICAN DIABETES ASSOCIATION 2014. Diagnosis and classification of diabetes mellitus. *Diabetes Care,* 37 Suppl 1**,** S81-90.

BANKS, P. A., BOLLEN, T. L., DERVENIS, C., GOOSZEN, H. G., JOHNSON, C. D., SARR, M. G., TSIOTOS, G. G. & VEGE, S. S. 2013. Classification of acute pancreatitis--2012: revision of the Atlanta classification and definitions by international consensus. *Gut,* 62**,** 102-11.

BANKS, P. A., CONWELL, D. L. & TOSKES, P. P. 2010. The management of acute and chronic pancreatitis. *Gastroenterology & hepatology,* 6**,** 1-16.

BATRA, J., SZABO, A., CAULFIELD, T. R., SOARES, A. S., SAHIN-TOTH, M. & RADISKY, E. S. 2013. Long-range electrostatic complementarity governs substrate recognition by human chymotrypsin C, a key regulator of digestive enzyme activation. *J Biol Chem,* 288**,** 9848-59.

BECK, J. A., LLOYD, S., HAFEZPARAST, M., LENNON-PIERCE, M., EPPIG, J. T., FESTING, M. F. W. & FISHER, E. M. C. 2000. Genealogies of mouse inbred strains. *Nature Genetics,* 24**,** 23-25.

BENAVIDES, F., RÜLICKE, T., PRINS, J.-B., BUSSELL, J., SCAVIZZI, F., CINELLI, P., HERAULT, Y. & WEDEKIND, D. 2019. Genetic quality assurance and genetic monitoring of laboratory mice and rats: FELASA Working Group Report. *Laboratory Animals,* 54**,** 135-148.

BLACKBERG, L., BLIND, P. J., LJUNGBERG, B. & HERNELL, O. 1985. On the source of bile salt-stimulated lipase in human milk: a study based on serum concentrations as determined by sandwich enzyme-linked immunosorbent assay technique. *J Pediatr Gastroenterol Nutr,* 4**,** 441-5.

BLUESTONE, J. A., HEROLD, K. & EISENBARTH, G. 2010. Genetics, pathogenesis and clinical interventions in type 1 diabetes. *Nature,* 464**,** 1293-300.

BONAL, C., THOREL, F., AIT-LOUNIS, A., REITH, W., TRUMPP, A. & HERRERA, P. L. 2009. Pancreatic Inactivation of c-Myc Decreases Acinar Mass and Transdifferentiates Acinar Cells Into Adipocytes in Mice. *Gastroenterology,* 136**,** 309-319.e9.

BOUABE, H. & OKKENHAUG, K. 2013. Gene targeting in mice: a review. *Methods in molecular biology (Clifton, N.J.),* 1064**,** 315-336.

BRAYER, G. D., LUO, Y. & WITHERS, S. G. 1995. The structure of human pancreatic alpha-amylase at 1.8 A resolution and comparisons with related enzymes. *Protein Sci,* 4**,** 1730-42.

BRUNEAU, N. & LOMBARDO, D. 1995. Chaperone function of a Grp 94-related protein for folding and transport of the pancreatic bile salt-dependent lipase. *J Biol Chem,* 270**,** 13524-33.

BRUNEAU, N., NGANGA, A., FISHER, E. A. & LOMBARDO, D. 1997. O-Glycosylation of C-terminal tandem-repeated sequences regulates the secretion of rat pancreatic bile salt-dependent lipase. *J Biol Chem,* 272**,** 27353-61.

CHATILA, A. T., BILAL, M. & GUTURU, P. 2019. Evaluation and management of acute pancreatitis. *World journal of clinical cases,* 7**,** 1006-1020.

CHEN, X. 2018. *Protein Composition and Biogenesis of the Pancreatic Zymogen Granules* [Online]. Pancreapedia: Exocrine Pancreas Knowledge Base. Available: https://www.pancreapedia.org/reviews/protein-composition-and-biogenesis-of-pancreatic-zymogen-granules [Accessed].

CHUVIN, N., VINCENT, D. F., POMMIER, R. M., ALCARAZ, L. B., GOUT, J., CALIGARIS, C., YACOUB, K., CARDOT, V., ROGER, E., KANIEWSKI, B., MARTEL, S., CINTAS, C., GODDARD-LÉON, S., COLOMBE, A., VALANTIN, J., GADOT, N., SERVOZ, E., MORTON, J., GODDARD, I., COUVELARD, A., REBOURS, V., GUILLERMET, J., SANSOM, O. J., TREILLEUX, I., VALCOURT, U., SENTIS, S., DUBUS, P. & BARTHOLIN, L. 2017. Acinar-to-Ductal Metaplasia Induced by Transforming Growth Factor Beta Facilitates

KRAS(G12D)-driven Pancreatic Tumorigenesis. *Cellular and molecular gastroenterology and hepatology,* 4**,** 263-282.
CONCANNON, P., RICH, S. S. & NEPOM, G. T. 2009. Genetics of Type 1A Diabetes. *New England Journal of Medicine,* 360**,** 1646-1654.
COPSTEAD, L.-E. & BANASIK, J. 2013. *Pathophysiology*, Elsevier.
COULIER, B. 2016. Pancreatic Lipomatosis: An Extensive Pictorial Review. *Journal of the Belgian Society of Radiology,* 100**,** 39-39.
DALVA, M., EL JELLAS, K., STEINE, S. J., JOHANSSON, B. B., RINGDAL, M., TORSVIK, J., IMMERVOLL, H., HOEM, D., LAEMMERHIRT, F., SIMON, P., LERCH, M. M., JOHANSSON, S., NJOLSTAD, P. R., WEISS, F. U., FJELD, K. & MOLVEN, A. 2017. Copy number variants and VNTR length polymorphisms of the carboxyl-ester lipase (CEL) gene as risk factors in pancreatic cancer. *Pancreatology,* 17**,** 83-88.
DALVA, M., LAVIK, I. K., EL JELLAS, K., GRAVDAL, A., LUGEA, A., PANDOL, S. J., NJØLSTAD, P. R., WALDRON, R. T., FJELD, K., JOHANSSON, B. B. & MOLVEN, A. 2020. Pathogenic Carboxyl Ester Lipase (CEL) Variants Interact with the Normal CEL Protein in Pancreatic Cells. *Cells,* 9**,** 244.
DHAR, P., KALGHATGI, S. & SARAF, V. 2015. Pancreatic cancer in chronic pancreatitis. *Indian journal of surgical oncology,* 6**,** 57-62.
EL JELLAS, K., JOHANSSON, B. B., FJELD, K., ANTONOPOULOS, A., IMMERVOLL, H., CHOI, M. H., HOEM, D., LOWE, M. E., LOMBARDO, D., NJOLSTAD, P. R., DELL, A., MAS, E., HASLAM, S. M. & MOLVEN, A. 2018. The mucinous domain of pancreatic carboxyl-ester lipase (CEL) contains core 1/core 2 O-glycans that can be modified by ABO blood group determinants. *J Biol Chem,* 293**,** 19476-19491.
ETEMAD, B. & WHITCOMB, D. C. 2001. Chronic pancreatitis: diagnosis, classification, and new genetic developments. *Gastroenterology,* 120**,** 682-707.
EYDOUX, C., SPINELLI, S., DAVIS, T. L., WALKER, J. R., SEITOVA, A., DHE-PAGANON, S., DE CARO, A., CAMBILLAU, C. & CARRIERE, F. 2008. Structure of human pancreatic lipase-related protein 2 with the lid in an open conformation. *Biochemistry,* 47**,** 9553-64.
FISHER-WELLMAN, K. H., RYAN, T. E., SMITH, C. D., GILLIAM, L. A. A., LIN, C.-T., REESE, L. R., TORRES, M. J. & NEUFER, P. D. 2016. A Direct Comparison of Metabolic Responses to High-Fat Diet in C57BL/6J and C57BL/6NJ Mice. *Diabetes,* 65**,** 3249-3261.
FJELD, K., WEISS, F. U., LASHER, D., ROSENDAHL, J., CHEN, J.-M., JOHANSSON, B. B., KIRSTEN, H., RUFFERT, C., MASSON, E., STEINE, S. J., BUGERT, P., CNOP, M., GRÜTZMANN, R., MAYERLE, J., MÖSSNER, J., RINGDAL, M., SCHULZ, H.-U., SENDLER, M., SIMON, P., SZTROMWASSER, P., TORSVIK, J., SCHOLZ, M., TJORA, E., FÉREC, C., WITT, H., LERCH, M. M., NJØLSTAD, P. R., JOHANSSON, S. & MOLVEN, A. 2015. A recombined allele of the lipase gene CEL and its pseudogene CELP confers susceptibility to chronic pancreatitis. *Nature genetics,* 47**,** 518-522.
GEISZ, A. & SAHIN-TÓTH, M. 2018. A preclinical model of chronic pancreatitis driven by trypsinogen autoactivation. *Nature Communications,* 9**,** 5033.
GOYAL, R. & JIALAL, I. 2020. *Diabetes Mellitus Type 2* [Online]. StatPearls. Available: https://www.ncbi.nlm.nih.gov/books/NBK513253/ [Accessed].
GUDGEON, A. M., PATEL, G., HERMON-TAYLOR, J., HURLEY, P., BOWYER, R. C. & JEHANLI, A. M. 1991. Detection of human pancreatic pro-phospholipase A2 activation using an immunoassay for the free activation peptide DSGISPR. *Ann Clin Biochem,* 28 (Pt 5)**,** 497-503.
GURUMURTHY, C. B. & LLOYD, K. C. K. 2019. Generating mouse models for biomedical research: technological advances. *Disease models & mechanisms,* 12**,** dmm029462.
HAMADA, S., MASAMUNE, A. & SHIMOSEGAWA, T. 2015. *Pancreatic fibrosis* [Online]. Pancreapedia: Exocrine Pancreas Knowledge Base. Available: https://www.pancreapedia.org/reviews/pancreatic-fibrosis [Accessed].
HEGYI, E. & SAHIN-TÓTH, M. 2017. Genetic Risk in Chronic Pancreatitis: The Trypsin-Dependent Pathway. *Digestive diseases and sciences,* 62**,** 1692-1701.
HEGYI, E. & SAHIN-TÓTH, M. 2019. Human CPA1 mutation causes digestive enzyme misfolding and chronic pancreatitis in mice. *Gut,* 68**,** 301-312.
HEGYI, P., PÁRNICZKY, A., LERCH, M. M., SHEEL, A. R. G., REBOURS, V., FORSMARK, C. E., DEL CHIARO, M., ROSENDAHL, J., DE-MADARIA, E., SZÜCS, Á., TAKAORI, K., YADAV, D., GHEORGHE, C., RAKONCZAY, Z., MOLERO, X., INUI, K., MASAMUNE, A., FERNANDEZ-DEL CASTILLO, C., SHIMOSEGAWA, T.,

NEOPTOLEMOS, J. P., WHITCOMB, D. C. & SAHIN-TÓTH, M. 2020. International Consensus Guidelines for Risk Factors in Chronic Pancreatitis. Recommendations from the working group for the international consensus guidelines for chronic pancreatitis in collaboration with the International Association of Pancreatology, the American Pancreatic Association, the Japan Pancreas Society, and European Pancreatic Club. *Pancreatology*.

HERNELL, O. & OLIVECRONA, T. 1974. Human milk lipases II. Bile salt-stimulated lipase. *Biochimica et Biophysica Acta (BBA) - Lipids and Lipid Metabolism,* 369**,** 234-244.

HESSMANN, E., ZHANG, J.-S., CHEN, N.-M., HASSELLUHN, M., LIOU, G.-Y., STORZ, P., ELLENRIEDER, V., BILLADEAU, D. D. & KOENIG, A. 2016. NFATc4 Regulates Sox9 Gene Expression in Acinar Cell Plasticity and Pancreatic Cancer Initiation. *Stem cells international,* 2016**,** 5272498-5272498.

HETZ, C. 2012. The unfolded protein response: controlling cell fate decisions under ER stress and beyond. *Nature Reviews Molecular Cell Biology,* 13**,** 89-102.

HIDALGO, M., CASCINU, S., KLEEFF, J., LABIANCA, R., LÖHR, J. M., NEOPTOLEMOS, J., REAL, F. X., VAN LAETHEM, J.-L. & HEINEMANN, V. 2015. Addressing the challenges of pancreatic cancer: Future directions for improving outcomes. *Pancreatology,* 15**,** 8-18.

HIGUCHI, S., NAKAMURA, Y. & SAITO, S. 2002. Characterization of a VNTR polymorphism in the coding region of the CEL gene. *J Hum Genet,* 47**,** 213-5.

HOLMES, R. S. & COX, L. A. 2011. Comparative Structures and Evolution of Vertebrate Carboxyl Ester Lipase (CEL) Genes and Proteins with a Major Role in Reverse Cholesterol Transport. *Cholesterol,* 2011**,** 781643-781643.

HOUSDEN, B. E., MUHAR, M., GEMBERLING, M., GERSBACH, C. A., STAINIER, D. Y. R., SEYDOUX, G., MOHR, S. E., ZUBER, J. & PERRIMON, N. 2017. Loss-of-function genetic tools for animal models: cross-species and cross-platform differences. *Nature Reviews Genetics,* 18**,** 24-40.

IONESCU-TIRGOVISTE, C., GAGNIUC, P. A., GUBCEAC, E., MARDARE, L., POPESCU, I., DIMA, S. & MILITARU, M. 2015. A 3D map of the islet routes throughout the healthy human pancreas. *Scientific Reports,* 5**,** 14634.

IRGENS, H. U., MOLNES, J., JOHANSSON, B. B., RINGDAL, M., SKRIVARHAUG, T., UNDLIEN, D. E., SOVIK, O., JONER, G., MOLVEN, A. & NJOLSTAD, P. R. 2013. Prevalence of monogenic diabetes in the population-based Norwegian Childhood Diabetes Registry. *Diabetologia,* 56**,** 1512-9.

ISHII, A., KUROSAWA, A., SAITO, S. & ADACHI, N. 2014. Analysis of the role of homology arms in gene-targeting vectors in human cells. *PloS one,* 9**,** e108236-e108236.

JIANG, G. & ZHANG, B. B. 2003. Glucagon and regulation of glucose metabolism. *American Journal of Physiology-Endocrinology and Metabolism,* 284**,** E671-E678.

JOHANSSON, B. B., FJELD, K., EL JELLAS, K., GRAVDAL, A., DALVA, M., TJORA, E., RAEDER, H., KULKARNI, R. N., JOHANSSON, S., NJOLSTAD, P. R. & MOLVEN, A. 2018. The role of the carboxyl ester lipase (CEL) gene in pancreatic disease. *Pancreatology,* 18**,** 12-19.

JOHANSSON, B. B., TORSVIK, J., BJØRKHAUG, L., VESTERHUS, M., RAGVIN, A., TJORA, E., FJELD, K., HOEM, D., JOHANSSON, S., RÆDER, H., LINDQUIST, S., HERNELL, O., CNOP, M., SARASTE, J., FLATMARK, T., MOLVEN, A. & NJØLSTAD, P. R. 2011. Diabetes and pancreatic exocrine dysfunction due to mutations in the carboxyl ester lipase gene-maturity onset diabetes of the young (CEL-MODY): a protein misfolding disease. *The Journal of biological chemistry,* 286**,** 34593-34605.

JUN, I., LEE, M. G. & MUALLEM, S. 2016. *Molecular Mechanisms of Pancreatic Bicarbonate Secretion* [Online]. Pancreapedia: Exocrine Pancreas Knowledge Base. Available: https://www.pancreapedia.org/node/9789 [Accessed].

KAVVOURA, F. K. & OWEN, K. R. 2019. Monogenic diabetes. *Medicine,* 47**,** 16-21.

KHARROUBI, A. T. & DARWISH, H. M. 2015. Diabetes mellitus: The epidemic of the century. *World journal of diabetes,* 6**,** 850-867.

KIM, H.-S. & LEE, M.-K. 2016. β-Cell regeneration through the transdifferentiation of pancreatic cells: Pancreatic progenitor cells in the pancreas. *Journal of Diabetes Investigation,* 7**,** 286-296.

KOLAR, M. J., KAMAT, S. S., PARSONS, W. H., HOMAN, E. A., MAHER, T., PERONI, O. D., SYED, I., FJELD, K., MOLVEN, A., KAHN, B. B., CRAVATT, B. F. & SAGHATELIAN, A. 2016. Branched Fatty Acid Esters of Hydroxy Fatty Acids Are Preferred Substrates of the MODY8 Protein Carboxyl Ester Lipase. *Biochemistry,* 55**,** 4636-4641.

KUMAR, T. R., LARSON, M., WANG, H., MCDERMOTT, J. & BRONSHTEYN, I. 2009. Transgenic mouse technology: principles and methods. *Methods in molecular biology (Clifton, N.J.),* 590**,** 335-362.

LAETHEM, R. M., BLUMENKOPF, T. A., CORY, M., ELWELL, L., MOXHAM, C. P., RAY, P. H., WALTON, L. M. & SMITH, G. K. 1996. Expression and Characterization of Human Pancreatic Preprocarboxypeptidase A1 and Preprocarboxypeptidase A2. *Archives of Biochemistry and Biophysics,* 332**,** 8-18.

LIDBERG, U., NILSSON, J., STROMBERG, K., STENMAN, G., SAHLIN, P., ENERBACK, S. & BJURSELL, G. 1992. Genomic organization, sequence analysis, and chromosomal localization of the human carboxyl ester lipase (CEL) gene and a CEL-like (CELL) gene. *Genomics,* 13**,** 630-40.

LINDQUIST, S. & HERNELL, O. 2010. Lipid digestion and absorption in early life: an update. *Curr Opin Clin Nutr Metab Care,* 13**,** 314-20.

LIU, J., AKANUMA, N., LIU, C., NAJI, A., HALFF, G. A., WASHBURN, W. K., SUN, L. & WANG, P. 2016. TGF-β1 promotes acinar to ductal metaplasia of human pancreatic acinar cells. *Scientific Reports,* 6**,** 30904.

LOMBARDO, D. 2001. Bile salt-dependent lipase: its pathophysiological implications. *Biochim Biophys Acta,* 1533**,** 1-28.

LOMBARDO, D. & GUY, O. 1980. Studies on the substrate specificity of a carboxyl ester hydrolase from human pancreatic juice. II. Action on cholesterol esters and lipid-soluble vitamin esters. *Biochimica et Biophysica Acta (BBA) - Enzymology,* 611**,** 147-155.

LOMBARDO, D., GUY, O. & FIGARELLA, C. 1978. Purification and characterization of a carboxyl ester hydrolase from human pancreatic juice. *Biochimica et Biophysica Acta (BBA) - Enzymology,* 527**,** 142-149.

LONGNECKER, D. S. 2014. Anatomy and Histology of the Pancreas. 1 ed. Pancreapedia: Exocrine Pancreas Knowledge Base.

LOWE, M. E. 1997. Molecular mechanisms of rat and human pancreatic triglyceride lipases. *J Nutr,* 127**,** 549-57.

MAAHS, D. M., WEST, N. A., LAWRENCE, J. M. & MAYER-DAVIS, E. J. 2010. Epidemiology of type 1 diabetes. *Endocrinology and metabolism clinics of North America,* 39**,** 481-497.

MADEYSKI, K., LIDBERG, U., BJURSELL, G. & NILSSON, J. 1999. Characterization of the gorilla carboxyl ester lipase locus, and the appearance of the carboxyl ester lipase pseudogene during primate evolution. *Gene,* 239**,** 273-82.

MADOLE, M. B., IYER, C. M., MADIVALAR, M. T., WADDE, S. K. & HOWALE, D. S. 2016. Evaluation of Biochemical Markers Serum Amylase and Serum Lipase for the Assessment of Pancreatic Exocrine Function in Diabetes Mellitus. *Journal of clinical and diagnostic research : JCDR,* 10**,** BC01-BC04.

MAJUMDER, S., PHILIP, N. A., TAKAHASHI, N., LEVY, M. J., SINGH, V. P. & CHARI, S. T. 2017. Fatty Pancreas: Should We Be Concerned? *Pancreas,* 46**,** 1251-1258.

MANN, E. & BELLIN, M. D. 2016. *Secretion of Insulin in Response to Diet and Hormones* [Online]. Pancreapedia: Exocrine Pancreas Knowledge Base. [Accessed].

MATTHEWS, E. K., PETERSEN, O. H. & WILLIAMS, J. A. 1973. Pancreatic acinar cells: acetylcholine-induced membrane depolarization, calcium efflux and amylase release. *The Journal of physiology,* 234**,** 689-701.

MAYERLE, J., SENDLER, M., HEGYI, E., BEYER, G., LERCH, M. M. & SAHIN-TOTH, M. 2019. Genetics, Cell Biology, and Pathophysiology of Pancreatitis. *Gastroenterology,* 156**,** 1951-1968.e1.

MOLVEN, A. & NJOLSTAD, P. R. 2011. Role of molecular genetics in transforming diagnosis of diabetes mellitus. *Expert Rev Mol Diagn,* 11**,** 313-20.

MOTTA, P. M., MACCHIARELLI, G., NOTTOLA, S. A. & CORRER, S. 1997. Histology of the exocrine pancreas. *Microsc Res Tech,* 37**,** 384-98.

MUNIRAJ, T., ASLANIAN, H. R., FARRELL, J. & JAMIDAR, P. A. 2014. Chronic pancreatitis, a comprehensive review and update. Part I: epidemiology, etiology, risk factors, genetics, pathophysiology, and clinical features. *Dis Mon,* 60**,** 530-50.

MURAKAMI, T. & FUJITA, T. 1992. Microcirculation of the rat pancreas, with special reference to the insulo-acinar portal and insulo-venous drainage systems: a further scanning electron microscope study of corrosion casts. *Arch Histol Cytol,* 55**,** 453-76.

MURTAUGH, L. C. & KEEFE, M. D. 2015. Regeneration and repair of the exocrine pancreas. *Annu Rev Physiol,* 77**,** 229-49.

NILSSON, J., HELLQUIST, M. & BJURSELL, G. 1993. The human carboxyl ester lipase-like (CELL) gene is ubiquitously expressed and contains a hypervariable region. *Genomics,* 17**,** 416-22.

ORTH, M., METZGER, P., GERUM, S., MAYERLE, J., SCHNEIDER, G., BELKA, C., SCHNURR, M. & LAUBER, K. 2019. Pancreatic ductal adenocarcinoma: biological hallmarks, current status, and future perspectives of combined modality treatment approaches. *Radiation oncology (London, England),* 14**,** 141-141.

PANDIRI, A. R. 2014. Overview of exocrine pancreatic pathobiology. *Toxicol Pathol,* 42**,** 207-16.

PASQUALINI, E., CAILLOL, N., VALETTE, A., LLOUBES, R., VERINE, A. & LOMBARDO, D. 2000. Phosphorylation of the rat pancreatic bile-salt-dependent lipase by casein kinase II is essential for secretion. *Biochem J,* 345 Pt 1**,** 121-8.

PERLMAN, R. L. 2016. Mouse models of human disease: An evolutionary perspective. *Evolution, medicine, and public health,* 2016**,** 170-176.

PHAM, A. & FORSMARK, C. 2018. Chronic pancreatitis: review and update of etiology, risk factors, and management. *F1000Res,* 7.

PHIFER-RIXEY, M. & NACHMAN, M. W. 2015. Insights into mammalian biology from the wild house mouse Mus musculus. *eLife,* 4**,** e05959.

PULGARON, E. R. & DELAMATER, A. M. 2014. Obesity and type 2 diabetes in children: epidemiology and treatment. *Current diabetes reports,* 14**,** 508-508.

RAWLA, P., SUNKARA, T. & GADUPUTI, V. 2019. Epidemiology of Pancreatic Cancer: Global Trends, Etiology and Risk Factors. *World journal of oncology,* 10**,** 10-27.

ROGERS, S., WELLS, R. & RECHSTEINER, M. 1986. Amino Acid Sequences Common to Rapidly Degraded Proteins: The PEST Hypothesis. *Science,* 234**,** 364-368.

RÆDER, H., HALDORSEN, I. S., ERSLAND, L., GRUNER, R., TAXT, T., SOVIK, O., MOLVEN, A. & NJOLSTAD, P. R. 2007. Pancreatic lipomatosis is a structural marker in nondiabetic children with mutations in carboxyl-ester lipase. *Diabetes,* 56**,** 444-9.

RÆDER, H., JOHANSSON, S., HOLM, P. I., HALDORSEN, I. S., MAS, E., SBARRA, V., NERMOEN, I., EIDE, S. Å., GREVLE, L., BJØRKHAUG, L., SAGEN, J. V., AKSNES, L., SØVIK, O., LOMBARDO, D., MOLVEN, A. & NJØLSTAD, P. R. 2006. Mutations in the CEL VNTR cause a syndrome of diabetes and pancreatic exocrine dysfunction. *Nature Genetics,* 38**,** 54-62.

RÆDER, H., MCALLISTER, F. E., TJORA, E., BHATT, S., HALDORSEN, I., HU, J., WILLEMS, S. M., VESTERHUS, M., EL OUAAMARI, A., LIU, M., RAEDER, M. B., IMMERVOLL, H., HOEM, D., DIMCEVSKI, G., NJOLSTAD, P. R., MOLVEN, A., GYGI, S. P. & KULKARNI, R. N. 2014. Carboxyl-ester lipase maturity-onset diabetes of the young is associated with development of pancreatic cysts and upregulated MAPK signaling in secretin-stimulated duodenal fluid. *Diabetes,* 63**,** 259-69.

RÆDER, H., VESTERHUS, M., EL OUAAMARI, A., PAULO, J. A., MCALLISTER, F. E., LIEW, C. W., HU, J., KAWAMORI, D., MOLVEN, A., GYGI, S. P., NJOLSTAD, P. R., KAHN, C. R. & KULKARNI, R. N. 2013. Absence of diabetes and pancreatic exocrine dysfunction in a transgenic model of carboxyl-ester lipase-MODY (maturity-onset diabetes of the young). *PLoS One,* 8**,** e60229.

SAHIN-TOTH, M. 2017. Genetic risk in chronic pancreatitis: the misfolding-dependent pathway. *Curr Opin Gastroenterol,* 33**,** 390-395.

SALOMAN, J. L., ALBERS, K. M., CRUZ-MONSERRATE, Z., DAVIS, B. M., EDDERKAOUI, M., EIBL, G., EPOUHE, A. Y., GEDEON, J. Y., GORELICK, F. S., GRIPPO, P. J., GROBLEWSKI, G. E., HUSAIN, S. Z., LAI, K. K. Y., PANDOL, S. J., UC, A., WEN, L. & WHITCOMB, D. C. 2019. Animal Models: Challenges and Opportunities to Determine Optimal Experimental Models of Pancreatitis and Pancreatic Cancer. *Pancreas,* 48**,** 759-779.

SCHEELE, G., BARTELT, D. & BIEGER, W. 1981. Characterization of human exocrine pancreatic proteins by two-dimensional isoelectric focusing/sodium dodecyl sulfate gel electrophoresis. *Gastroenterology,* 80**,** 461-73.

SCHMITZ, M. L., SHABAN, M. S., ALBERT, B. V., GÖKÇEN, A. & KRACHT, M. 2018. The Crosstalk of Endoplasmic Reticulum (ER) Stress Pathways with NF-κB: Complex Mechanisms Relevant for Cancer, Inflammation and Infection. *Biomedicines,* 6**,** 58.

SIEGEL, R. L., MILLER, K. D. & JEMAL, A. 2019. Cancer statistics, 2019. *CA Cancer J Clin,* 69**,** 7-34.

SIMON, M. M., GREENAWAY, S., WHITE, J. K., FUCHS, H., GAILUS-DURNER, V., WELLS, S., SORG, T., WONG, K., BEDU, E., CARTWRIGHT, E. J., DACQUIN, R., DJEBALI, S., ESTABEL, J., GRAW, J., INGHAM, N. J., JACKSON, I. J., LENGELING, A., MANDILLO, S., MARVEL, J., MEZIANE, H., PREITNER, F., PUK, O., ROUX, M., ADAMS, D. J., ATKINS, S., AYADI, A., BECKER, L., BLAKE, A., BROOKER, D., CATER, H., CHAMPY, M. F., COMBE, R., DANECEK, P., DI FENZA, A., GATES, H., GERDIN, A. K., GOLINI, E., HANCOCK, J. M., HANS, W., HOLTER, S. M., HOUGH, T., JURDIC, P., KEANE, T. M., MORGAN, H., MULLER, W., NEFF, F., NICHOLSON, G., PASCHE, B., ROBERSON, L. A., ROZMAN, J., SANDERSON, M., SANTOS, L., SELLOUM, M., SHANNON, C., SOUTHWELL, A., TOCCHINI-VALENTINI, G. P., VANCOLLIE, V. E., WESTERBERG, H., WURST, W., ZI, M., YALCIN, B., RAMIREZ-SOLIS, R., STEEL, K. P., MALLON, A. M., DE ANGELIS, M. H., HERAULT, Y. & BROWN, S. D. 2013. A comparative phenotypic and genomic analysis of C57BL/6J and C57BL/6N mouse strains. *Genome Biol,* 14**,** R82.

SZABÓ, A., PILSAK, C., BENCE, M., WITT, H. & SAHIN-TÓTH, M. 2016. Complex Formation of Human Proelastases with Procarboxypeptidases A1 and A2. *Journal of Biological Chemistry,* 291**,** 17706-17716.

TAYLOR, A. K., ZAMBAUX, J. L., KLISAK, I., MOHANDAS, T., SPARKES, R. S., SCHOTZ, M. C. & LUSIS, A. J. 1991. Carboxyl ester lipase: A highly polymorphic locus on human chromosome 9qter. *Genomics,* 10**,** 425-431.

TJORA, E., WATHLE, G., ENGJOM, T., ERCHINGER, F., MOLVEN, A., AKSNES, L., HALDORSEN, I. S., DIMCEVSKI, G., NJØLSTAD, P. R. & RÆDER, H. 2013. Severe Pancreatic Dysfunction But Compensated Nutritional Status in Monogenic Pancreatic Disease Caused by Carboxyl-Ester Lipase Mutations. *Pancreas,* 42.

TOMITA, N., IZUMOTO, Y., HORII, A., DOI, S., YOKOUCHI, H., OGAWA, M., MORI, T. & MATSUBARA, K. 1989. Molecular cloning and nucleotide sequence of human pancreatic prechymotrypsinogen cDNA. *Biochem Biophys Res Commun,* 158**,** 569-75.

TORSVIK, J., JOHANSSON, B. B., DALVA, M., MARIE, M., FJELD, K., JOHANSSON, S., BJØRKØY, G., SARASTE, J., NJØLSTAD, P. R. & MOLVEN, A. 2014. Endocytosis of secreted carboxyl ester lipase in a syndrome of diabetes and pancreatic exocrine dysfunction. *The Journal of biological chemistry,* 289**,** 29097-29111.

TORSVIK, J., JOHANSSON, S., JOHANSEN, A., EK, J., MINTON, J., RAEDER, H., ELLARD, S., HATTERSLEY, A., PEDERSEN, O., HANSEN, T., MOLVEN, A. & NJOLSTAD, P. R. 2010. Mutations in the VNTR of the carboxyl-ester lipase gene (CEL) are a rare cause of monogenic diabetes. *Hum Genet,* 127**,** 55-64.

TROY, L. M. & MAXIM, S. P. 2018. The rise of genetically engineered mouse models of pancreatitis: A review of literature. *Biomolecular Concepts,* 9**,** 103-114.

URAKAMI, T. 2019. Maturity-onset diabetes of the young (MODY): current perspectives on diagnosis and treatment. *Diabetes, metabolic syndrome and obesity : targets and therapy,* 12**,** 1047-1056.

VESTERHUS, M., RAEDER, H., KURPAD, A. J., KAWAMORI, D., MOLVEN, A., KULKARNI, R. N., KAHN, C. R. & NJØLSTAD, P. R. 2010. Pancreatic function in carboxyl-ester lipase knockout mice. *Pancreatology : official journal of the International Association of Pancreatology (IAP) ... [et al.],* 10**,** 467-476.

WANG, C. S., DASHTI, A., JACKSON, K. W., YEH, J. C., CUMMINGS, R. D. & TANG, J. 1995. Isolation and characterization of human milk bile salt-activated lipase C-tail fragment. *Biochemistry,* 34**,** 10639-44.

WANG, G.-J., GAO, C.-F., WEI, D., WANG, C. & DING, S.-Q. 2009. Acute pancreatitis: etiology and common pathogenesis. *World journal of gastroenterology,* 15**,** 1427-1430.

WHITCOMB, D. C. 2012. Genetics of alcoholic and nonalcoholic pancreatitis. *Current opinion in gastroenterology,* 28**,** 501-506.

WHITCOMB, D. C., GORRY, M. C., PRESTON, R. A., FUREY, W., SOSSENHEIMER, M. J., ULRICH, C. D., MARTIN, S. P., GATES, L. K., JR., AMANN, S. T., TOSKES, P. P., LIDDLE, R., MCGRATH, K., UOMO, G., POST, J. C. & EHRLICH, G. D. 1996. Hereditary pancreatitis is caused by a mutation in the cationic trypsinogen gene. *Nat Genet,* 14**,** 141-5.

WORLD HEALTH ORGANIZATION. 2016. *Global Report on Diabetes* [Online]. who.int. [Accessed].

XIAO, X., JONES, G., SEVILLA, W. A., STOLZ, D. B., MAGEE, K. E., HAUGHNEY, M., MUKHERJEE, A., WANG, Y. & LOWE, M. E. 2016. A Carboxyl Ester Lipase (CEL) Mutant Causes Chronic Pancreatitis by Forming Intracellular Aggregates That Activate Apoptosis. *The Journal of biological chemistry,* 291**,** 23224-23236.

XUE, R., JIA, K., WANG, J., YANG, L., WANG, Y., GAO, L. & HAO, J. 2018. A Rising Star in Pancreatic Diseases: Pancreatic Stellate Cells. *Frontiers in physiology,* 9**,** 754-754.

Appendix

Body weight development for mice at 3 months of age

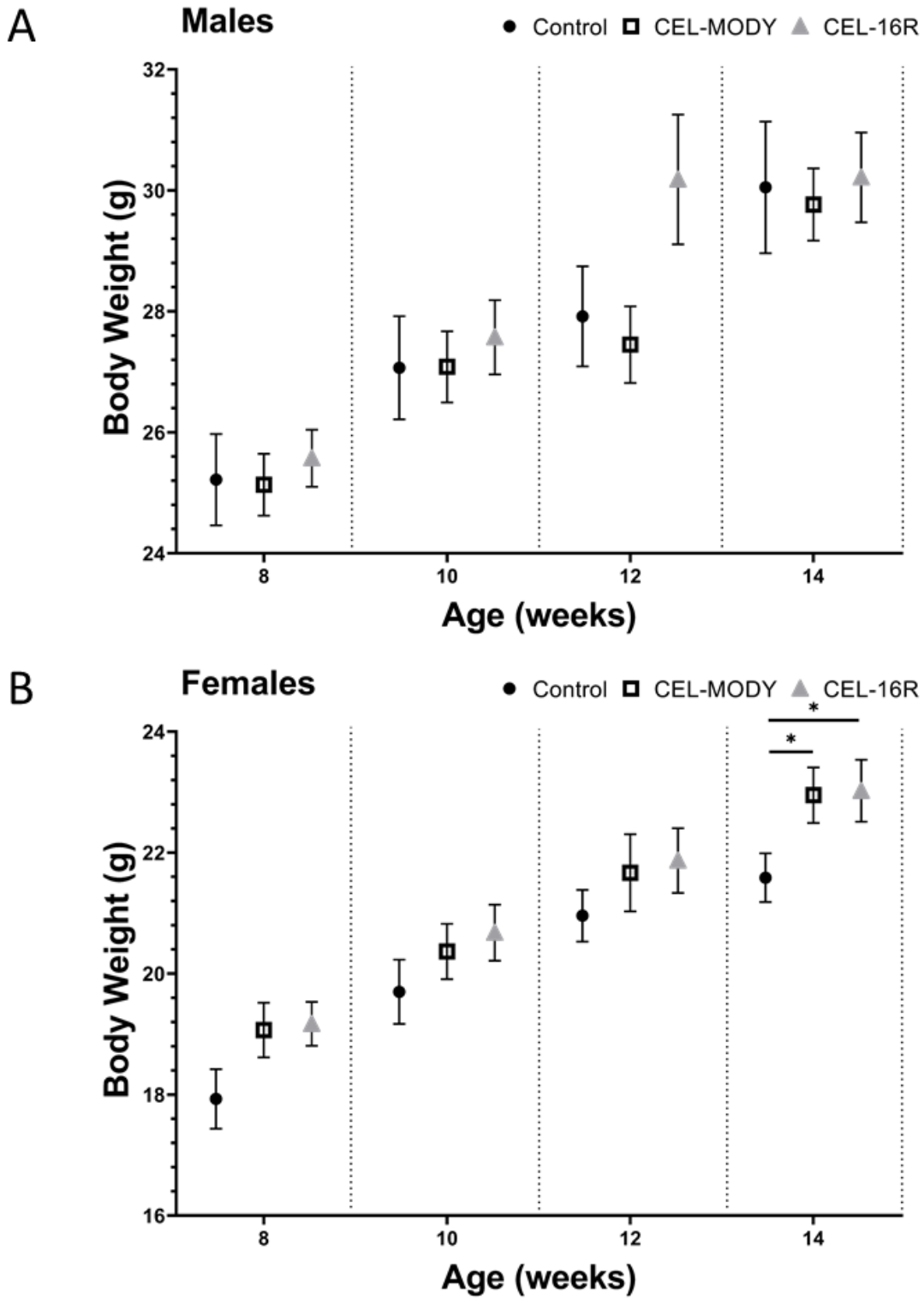

Figure 1. Body weight during life span of 3 months old CEL-MODY, CEL-16R and control mice. *The body weight (g) is presented as the mean at each age point for (A) males and (B) females. Error bars represent standard error of the mean. Statistical significance is indicated as * ($P < 0.05$). N=6-13.*

IPGTT for mice at 3 months of age

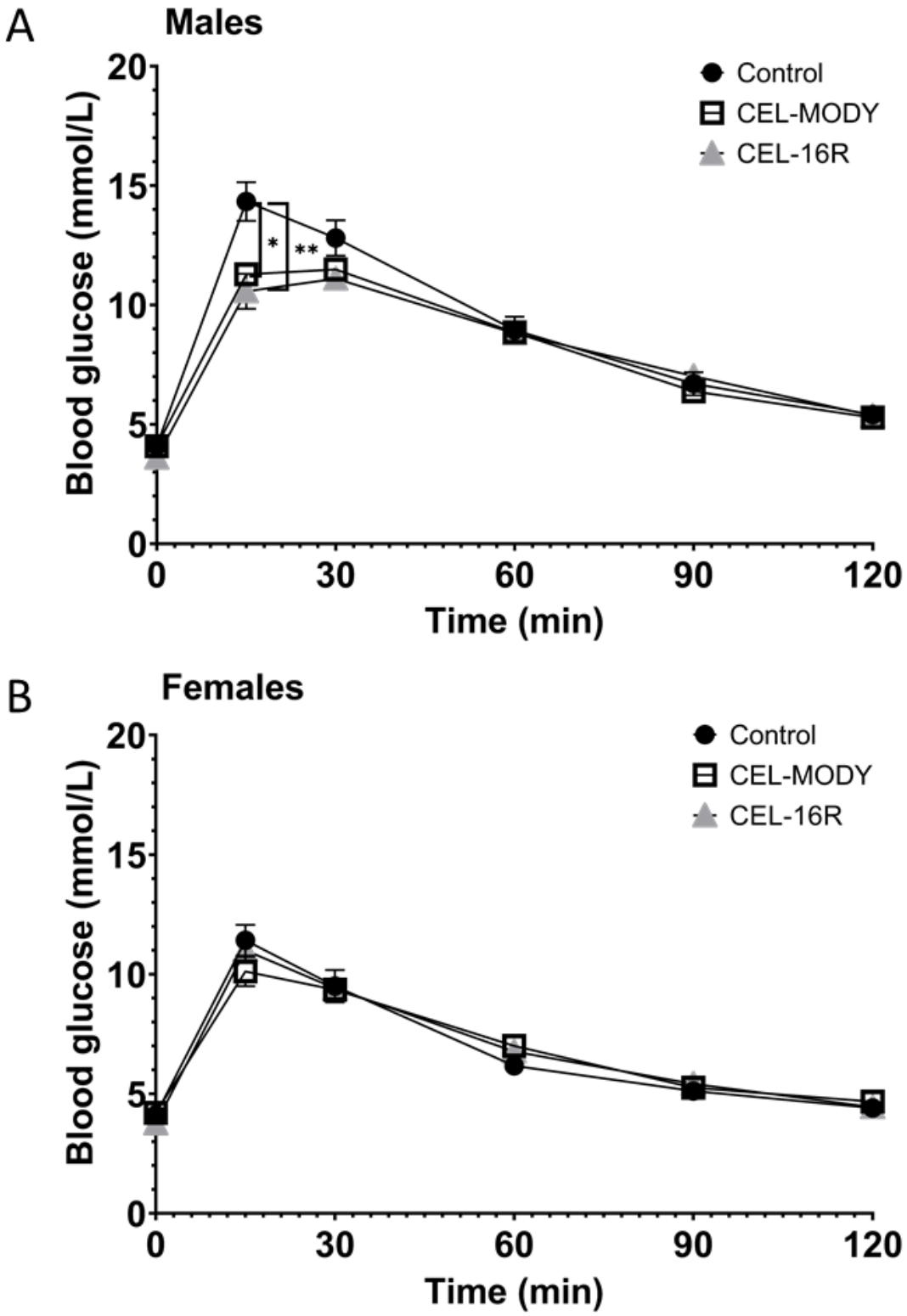

Figure 2. Intraperitoneal glucose tolerance test for 3 months old mice. *Time 0 represent blood glucose measurment before injection. CEL-MODY, CEL-16R and control mice are compared for (A) males and (B) females and represented with the mean for each strain. Error bar represent standard error of the mean. Statistical significance is indicated as * (P < 0.05) and ** (P < 0.01).*